Faculty of Aerospace Engineering

High-Speed Free-Flight Wind Tunnel Experiment With A Compromised Quadrotor

Creating A Dataset Suitable For Identification Of Aerodynamic Forces and Moments

Rudi Johannes Schilder

28 February 2019

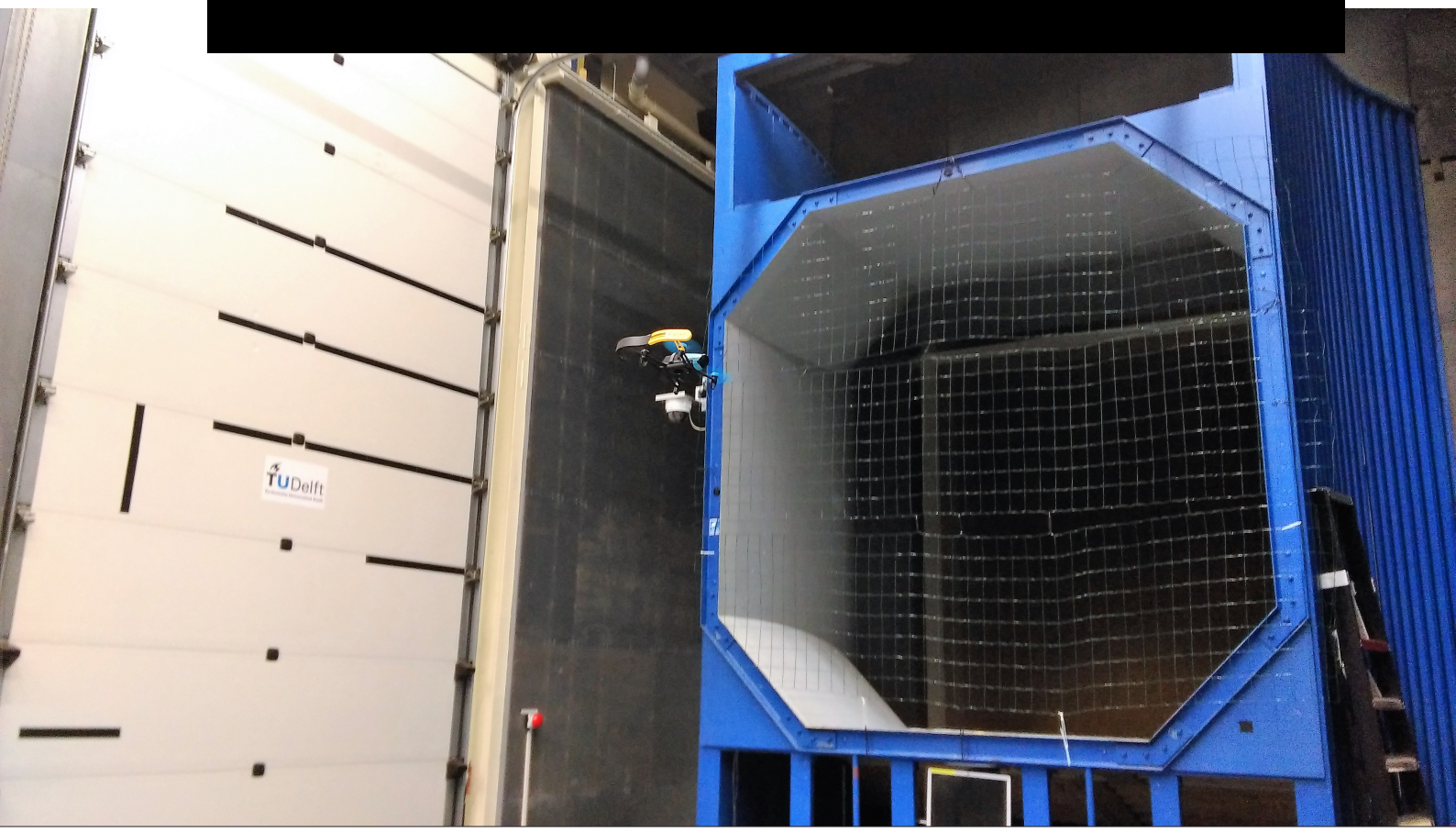

TU Delft Delft University of Technology

Challenge the future

High-Speed Free-Flight Wind Tunnel Experiment With A Compromised Quadrotor

Creating A Dataset Suitable For Identification Of Aerodynamic Forces and Moments

Master of Science Thesis

For obtaining the degree of Master of Science in Aerospace Engineering
at Delft University of Technology

Rudi Johannes Schilder

28 February 2019

Faculty of Aerospace Engineering · Delft University of Technology

Delft University of Technology

Delft University Of Technology
Department Of
Control and Simulation

The undersigned hereby certify that they have read and recommend to the Faculty of Aerospace Engineering for acceptance a thesis entitled **"High-Speed Free-Flight Wind Tunnel Experiment With A Compromised Quadrotor"** by **Rudi Johannes Schilder** in partial fulfillment of the requirements for the degree of **Master of Science**.

Dated: 28 February 2019

Readers:

dr.ir. C. C. de Visser

ir. S. Sun

dr.ir. Q. P. Chu

ir. R. Noomen

Acronyms

back-EMF	counter electromotive force
CFD	Computational Fluid Dynamics
C.G.	Center of Gravity
DOF	Degree of Freedom
EKF	Extended Kalman Filter
F&M	Forces & Moments
FRD	Forward-Right-Down
GPS	Global Position System
IMU	Inertial Measurement Unit
INDI	Incremental Nonlinear Dynamic Inversion
KF	Kalman Filter
LQR	Linear Quadratic Regression
LS	Least Squares
NDI	Nonlinear Dynamic Inversion
NED	North-East-Down
OJF	Open Jet Facility
TUDelft	Technical University of Delft
UAV	Unmanned Aerial Vehicle
UKF	Unscented Kalman Filter
VRS	Vortex Ring State
WLS	Weighted Least Squares

Contents

Summary

In the world of today, drones are receiving an ever increasing amount of recognition. Their rapid rise comes with an increasing demand for their reliability and safety. Should they ever be allowed to fly in great numbers around populated areas, fulfilling their wide range of uses, the requirements in safety will be strict.

As one of the most basic and widely used designs, the quadrotor or quadcopter has been the subject of an increasing body of research. Literature shows extensive effort being put in modeling, controlling, testing, and expanding their capabilities under tougher circumstances. This thesis seeks to show an existing gap in this field: the need for data driven models in high speed environments, while also experiencing limitations on control.

Fault tolerant controllers have been designed and tested to work with physical limitations on the rotors, without using extensive models, utilizing their high controllability. This fact allows quadrotors to handle new situations and controllers have demonstrated they optimize themselves as well. However, in order to fully predict their behavior in any circumstance, the existing models will need to be extended. These models are valid for the standard flight conditions. However, more extensive analysis is required near the edges of the flight envelope, and on the reduction of the flight envelope.

This thesis follows on the research goal set by the department of Guidance, Navigation & Control at the Technical University of Delft, to analyze flight envelopes and models and build a database for future reference. This thesis puts that goal into focus on the Parrot Bebop quadrotor and seeks to answer the following question.

How can the Parrot Bebop quadrotor dynamics be modeled for high-speed and single actuator loss conditions and identified from a free-flight wind tunnel experiment using modern system identification techniques?

This thesis presents the current state of the art and deduces the desired experiment and modeling approach that combined allows the research question to be answered. The current state of the art focuses on four main areas: quadrotor dynamics and modeling, sensor fusion and data gathering, fault tolerant control, and relevant system identification research.

The field of quadrotor modeling focuses on the established rigidbody kinematics model, with quadratic terms for the rotor forces. Often applied linear extensions include terms for drag

effects in all degrees of freedom. Extended and more substantiated models account for blade-flapping and the influx of wind on the rotors, resulting in non-nominal thrust. Other important factors are the wake interactions of the rotors, ground effect and lateral blade flapping forces.

The state of the art in the field of state estimation relies on the Extended Kalman Filter (EKF) to fuse onboard acceleration and gyroscopic data with the offboard position and attitude data from a OptiTrack motion camera system. Outstanding issues are the synchronization of sensors, the detection of outliers and filling gaps in the data.

Fault tolerant controllers have shown to be able to control quadrotors in the event of propeller faults. By releasing control of the yaw angle, the position can still be controlled. A Incremental Nonlinear Dynamic Inversion (INDI) controller was discovered that can combine sensor data and limited modeling to improve control behavior. The inclusion of both onboard learning and goal orientated control allocation have made this controller capable to handle high and low frequency disturbances and deal with propeller faults.

System identification in the field of quadrotors is seen as a relatively new field, with widely varying approaches and results. First, there is the white-box estimation of crucial parameters as inertia and actuator thrust, both from experiments and nonlinear optimization on flight data. Then, there is a variety of both time and frequency domain techniques, which are focused on estimating decoupled models useful for control. Lastly, there is also an increasing interest in predicting dynamics using black-box techniques such as neural networks, which is facilitated by the ease of access to flight data.

A variety of system identification tools remain also open, most notably multivariate spline modeling and stepwise regression analysis. With the expected amount of nonlinear behavior, multivariate splines are expected to handle this quite well, if enough data and a sufficient triangulation can be obtained. Stepwise regression analysis is a basic but very useful tool to gain insight in the dominant modes of the model and find better suited regression model structures.

The chosen approach is to conduct a wind tunnel test with five chosen cases. The chosen cases are: the baseline, a lost propeller, a reduced propeller effectiveness for two opposing propellers, the safety bumpers attached, and lastly, one safety bumper missing. During the experiment, control is handled by the Incremental Nonlinear Dynamic Inversion (INDI) controller, trained and tuned for each case. Data is gathered onboard and by the OptiTrack system, fused with an adaptation on the Extended Kalman Filter (EKF). The stepwise regression analysis is to be conducted in order to find force and moment model structures that explain the gathered data the best. The literature on quadrotor modeling will provide the basis on which suitable regressors will be chosen for the pool.

Paper

High-Speed Free-Flight Wind Tunnel Experiment With A Compromised Quadrotor

Rudi J. Schilder*, Sihao Sun†, and Coen C. de Visser‡
Faculty of Aerospace Engineering, Kluyverweg 1, 2629HS Delft, The Netherlands.

To aid in the continued effort of making unmanned flight safer, this paper presents the experimenting effort towards determining aerodynamic forces on a off-the-shelf quad-rotor under compromised circumstances. For the first time an Incremented Nonlinear Dynamic Inversion controller is used for compromised flight in wind tunnel conditions. For the Parrot Bebop v1, five aerodynamically different configurations were tested. These configurations include reduced rotor effectiveness on one or two rotors and the inclusion of one or two bumpers. In order to gather a suitable dataset for these highly dynamic models, free-flight model identification is deemed necessary.

To facilitate free-flight aerodynamic model identification, data was provided by the on-board inertial sensors and a motion-tracking OptiTrack system. Sensor fusion through Extended Kalman Filtering was chosen to counter frame vibrations and sensor bias. A sufficient convergence rate was found for estimating the biases. Further modeling efforts are required to validate these results. A rotor rate Kalman Filter was also designed to improve rotor rate differentiation.

Excitation of the system was performed with position-controlled doublets, designed to observe theoretical modes from existing quadrotor models. This resulted in five main types of excitation, designed to maximize yawing motions, thrust variation and drag effects. The differences seen for each configuration show interesting behavior, and further investigation is recommended.

The resulting dataset is considered uniquely suitable for estimating coupled dynamics with saturated actuators and loss of yaw control.

I. Introduction

Multirotor drones are becoming more and more popular with new applications emerging virtually every day. Small personal drones such as quadrotors will soon be an everyday occurrence. With a growing interest and usage due to their wide range of applications, incidents are more likely to occur and significant improvements in drone safety become a necessity.

With all these new additions to the airspace, requirements for drones will become stricter, especially if the tasks required are performed in urban environments. Drones will be expected to perform safely and accurately in high-end conditions. These include not only aggressive manoeuvres, high-speed winds and turbulence, but also resistance to damage due to any source. As such, when looking to the future, it is deemed vital to investigate drones under both high-speed and compromised circumstances, see for example [1].

A. State of the art

The quadrotor is one of the most widely used multirotor drones, and is the subject of this research. The motion of quadrotors has primarily been described by rigid body 6-DOF models experiencing a set of external forces and moments, where the aerodynamic effects play a key role. Rotors are the primary components that each generate a force and a moment. From literature that use helicopter based momentum theory and blade element theory, it can be concluded that at least three different phenomena have a significant effect. Firstly, the thrust is susceptible to the incoming flow velocity, especially during climbing and descending flight[2–4]. Secondly blade flapping occurs, resulting in an inclined rotor disk plane, producing a local drag force and elastic moment[4–6]. Thirdly hub force occurred due to induced drag produced by rotor blades[5].

*Graduate student, Control and Simulation, rudi.schilder@gmail.com
†Ph.D. student, Control and Simulation, s.sun-4@tudelft.nl, AIAA Member
‡Assistant professor, Control and Simulation, c.c.devisser@tudelft.nl, AIAA Member

Thrust variance model during climbing and descending flight are also successfully predicted by first principle approaches[2, 3]. However, due to the complexity of computing induced velocity and complex aerodynamic interactions between rotors, the existing first principle based model are unable to provide accurate thrust predictions in forward flight[3]. This is even more the case for coupled flight states in which lateral and longitudinal maneuver occur simultaneously.

In [7] a survey is conducted of system identification in the field of quadrotors. For the models presented in [7], what appears missing in the literature is a basis of experiments in free-flights, that establish globally valid models in a wide range of flight-envelope.

The contribution of this research is present a methodology for conducting experiments that enable system identification on quadrotors. The experiment methodology aims to cover high-speed free-flight, including under compromised circumstances.

B. Overview

The following sections, in order, present the research as it now stands. The models that are deemed suitable for future identification use are discussed in Section II. The resulting experiment and its design are discussed in Section III. The process used for filtering and state estimation is discussed in Section IV. A special focus is laid on the sensor fusion methods by means of Kalman filters. In Section V the resulting data is presented, with estimates of the final states and quality metrics. The final conclusions are given in Section VI.

II. Model structure setup

Kinematics, forces and moments modelling was done by assuming the drone as a rigid body structure. In reality the drone consists of two rigid bodies, that are connected through a spring-damper system. These are the rotor frame and the central body with the battery and flight computer. The dampers are installed to reduce high frequency movement of the central body, such that onboard sensors are less affected. For modeling purposes however, this is ignored. The vibrations are active at too small a timescale to be investigated, and assumed to be the result of imperfections that are difficult to measure.

In Section I.A it is established that there are a number of dominant aerodynamic forces that can be expected to act on the vehicle. Identifying, simulating and predicting these aerodynamics is the research aim. As such the expected aerodynamics have to be understood, allowing the experiment can be designed to observe these modes.

Equation 1 contains the kinematic equations of motion for a rigid body. The system for identification is then defined with Forces & Moments (F&M) as a function of the vehicle state and actuator inputs, i.e. $[\bar{F}, \bar{M}] = f(\bar{x}, \bar{\omega})$.

$$W \cdot \bar{g}_b + \bar{F} = m\dot{\bar{V}} + \bar{\Omega} \times \bar{V} \tag{1a}$$

$$\bar{M} = \mathbf{I} \cdot \dot{\bar{\Omega}} + \bar{\Omega} \times (\mathbf{I} \cdot \bar{\Omega}) \tag{1b}$$

The thrust produced by rotors is generally simplified to be a function of ω_i^2. However, even in simple models, biases can be seen, and when rotors are subjected to a moving flow, their effectiveness changes. For the case of forward flight, this is generally an increase in efficiency. For cases where the flow comes from beneath the rotor, i.e. in descent, the effect becomes separate into three distinct regions.

The Vortex Ring State (VRS) is an especially dangerous one, as the efficiency is drastically reduced, while also hard to model. This usually involves using probabilistic or approximations to the effect. It is also an often cited cause for crashes, since it decreases thrust during rapid descent, which can become unrecoverable. The effect becomes harder to study during sideways flight, as wake interaction is crucial to the VRS.

Wake modelling is found to be most effectively modelled as a function of the Angle of Attack (AoA) and it's derivative. With a small time delay, pitch and roll movements should induce extra forces when the wake of the body or attached bumpers interact with the rotors and vice versa.

Blade flapping is modelled as a change in the inclination of the rotor plane, away from the free stream velocity. This inclination is induced by the advancing and retreating of the blades in that experience asymmetric lift distributions during movement in the horizontal plane. Blade flapping is generally modelled as forces acting on the hub of a rotor (connecting point of rotor).

The remaining drag effects are often attributed to the induced drag of the blades and the parasitic drag of the body. The drag terms are often modelled as correlated to V. However, recently [8] has indicated that the parasitic drag in

most their cases is still correlated to V^2. Their tests include the high-speed region, using a F&M test rig in wind tunnel conditions.

III. Experiment setup and execution

To facilitate the future identification of the quadrotor aerodynamics, a wind tunnel experiment methodology was developed and implemented. The wind tunnel experiment of March 2017 is also described in [9]. The experiment was conducted for various configurations. However, in [9] the model identification is only aimed towards the baseline configuration, while multiple configurations were tested. As such this section is aimed to give a complete description of the experiment, and will not omit duplicate information.

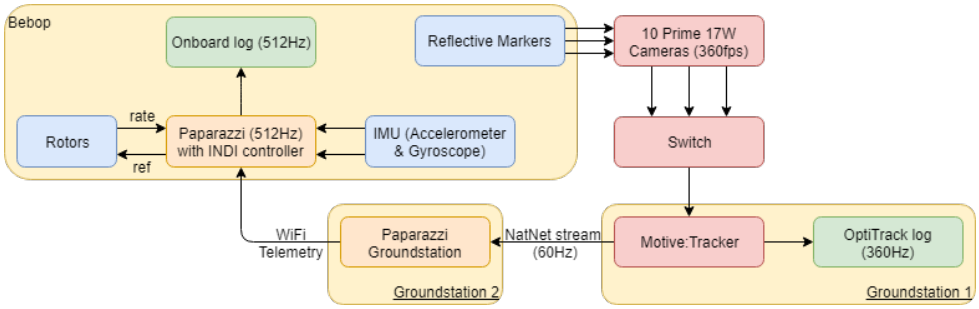

Fig. 1 Schematic of experimental setup

A. Parrot Bebop & onboard sensors

The Parrot Bebop 1 was selected as the off-the-shelf example of a quadrotor. The Bebop features brush-less rotors that can reach approximately 13 000 rpm during flight. It uses WiFi to connect with a control station, which can then send commands and information both ways. The commercial controller is replaced with Paparazzi UAV Autopilot. Paparazzi [10] is an open source autopilot maintained by researchers, including those from the Technological University of Delft.

The controller reads the sensors and commands the actuators at a frequency of 512Hz. For the purposes of this paper, this also sets the onboard sensor rate, even though they technically can acquire at even faster rates. The sensor data for identification is logged directly and filtered offline. The relevant onboard sensors are:

- A 3-axis accelerometer (MPU 6050).
- A 3-axis gyroscope (MPU 6050).
- Closed-loop brush-less rotors with counter-electromotive force (back-EMF) for rotor rate feedback & control.
- A 3-axis magnetometer (AKM 8963).

B. Experiment configurations

The quadrotor was tested with a variety of configurations. Firstly, the standard configuration has the quadrotor fly without any attachments or limitations.

The second consist of flights performed with one actuator partly damaged. This was simulated by reducing the radius of the propeller by 2 cm. This results in a theoretical flat reduction of the effectiveness by 40 %. The third configuration consisted of two opposing rotors being damaged for effectively 70 %. Modeling efforts will have to validate this estimated effectiveness reduction, for which comparison of these configurations is expected to help.

The fourth configuration attaches the bumpers on the sides. These act as protection for the propellers and objects in the vicinity of the quadrotor. These bumpers add significant aerodynamics, such as drag, wake interactions and destabilizing moments. The fifth configuration then simulates a quadrotor's structural damage to the casing by removing one of these bumpers. This single bumper case introduces very significant asymmetrical aerodynamic effects. Investigating this instability was selected as one of the suitable use cases for system identification.

Table 1 Experiment configurations of the Parrot Bebop.

Configuration	Explanation
Baseline	No limitations or additional features.
Single actuator 40	One propeller thrust reduced to 40 %, i.e. by 2 cm.
Two opposing actuators 70	Two opposing propeller radia reduced to 70 %, i.e. by 1 cm.
Bumpers	Two bumpers are attached on either side.
Left or right bumper	Single bumper attached to either left or right side.

C. Wind tunnel experiment setup

The Open Jet Facility (OJF) of the Technical University of Delft (TUDelft) is a wind tunnel facility capable of creating wind velocities of 35 m s^{-1}. Driven by a large fan, the flow is circulated through a wooden tunnel, guided by vanes around corners. Before entering the test section, the flow is smoothed by a set of a dense wire meshes and through a contraction enters the open test section. At the end of the test section stands a large cooler to control the temperature. A schematic can be found in Fig. 2a.

The test section is an open room where flow comes in from the wind tunnel outlet. The aperture has an octagonal cross section of 285 cm by 285 cm and is effectively 3 m in diameter. The outlet was covered by a mesh to protect it from uncontrolled behavior. This can be seen in Fig. 2b. The flow quality in the test section has been assessed prior by [11]. Lignarolo et al. state that the mean radial flow velocity at 1 m and 6 m is below 1% and 3%. Also the turbulence intensity in the test section is stated to be below 1% of the mean velocity. The test section itself diminishes in size, due to the shear layer expanding from the sides of the outlet with an dissipation angle of 9.5°.

The resulting usable test section is between 0.5 m and 6 m behind the outlet, with the usable cross section between 2.75 m and 2 m respectively. Only data points gathered inside the test section are considered. For each run the atmospheric conditions and flow velocity were logged and assumed constant during the flight.

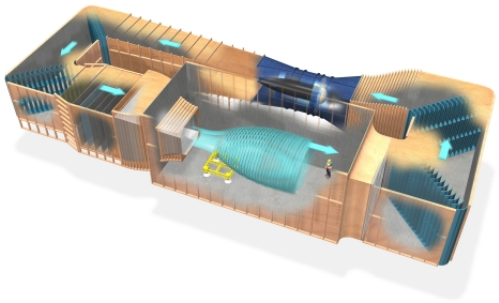

(a) Schematic of the OJF.

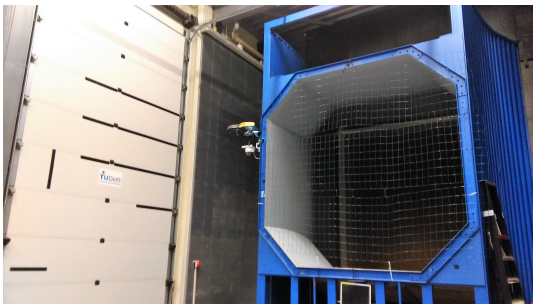

(b) Photo taken during the experiment, with the Bebop in single bumper configuration.

Fig. 2 The Open Jet Facility.

D. Data Acquisition and processing

External position and attitude sensing was provided by the OptiTrack motion tracking system. Markers were placed on each quadrotor, with their position in the body frame known.

The setup was as follows. Ten Prime 17W OptiTrack cameras were placed above and around the test section in a 4-2-4 pattern, facing in- and downward. They are capable of observing the position of a reflective marker in 2D at a rate of 360 Hz. Placed 7 m above the ground floor, the cameras are approximately 3.5 m above the ideal test height.

Overlapping arcs of 70° allowed for any marker to be visible to at least 4 cameras at any given time. Cameras were calibrated twice a day, using the process of wanding. The ground plane is set during this process and is leveled with respect to the gravity vector. The North vector is pointed towards the outlet, parallel with the direction of flow.

The cameras send their optical information through a server to a central computer running optical tracking software Motive 1.10.2. Motive combines the 2D data to establish the 3D marker positions and subsequently the position and attitude of the quadrotor, by assuming the markers are connected as a rigid body. During flight the OptiTrack data is published to the ground control station which informs the drone, allowing for OptiTrack data to serve as substitute for the Global Position System (GPS) and magnetometer. This allows for low latency position control ($t < 10$ ms).

The OptiTrack data is logged directly from Motive. Motive 1.10.2 post processing & reconstruction is applied on the OptiTrack data. The data tends to contain mislabeling errors, as well as false positives and complete gaps. Small gaps ($t < 0.1$ s) in individual marker data were interpolated linearly. With larger gaps, the marker's data is discarded and if insufficient markers are available for reconstruction, the rigid body is marked as untracked and the frame discarded.

The position and attitude logged by Motive represent the rigid body defined by markers, without knowledge of the actual vehicle. Before state estimation is performed, the information of the marker positions is used to establish a transformation of position and attitude data in the rigidbody frame to the body frame. The transform is determined by optimizing the position data of individual markers to the measured body frame positions of the markers for each individual quadrotor.

E. Quadrotor control & stabilization

During the experiments, the quadrotors were controlled by the Incremental Nonlinear Dynamic Inversion (INDI) controller as proposed by [12–14], with Weighted Least Squares (WLS) optimized control allocation. The addition of this controller allowed for hover (position) control to be augmented with improved attitude control on the inner loop. The INDI controller is more capable of dealing with heavy disturbances than the previous PID controller. The implemented controller was also allowed to learn online the control effectiveness, allowing for more control in continuous high-speed conditions

The onboard controller utilizes multiple loops for control. The drone was always controlled for position, for otherwise the drone would not be controllable in the heavy wind and counter intuitive conditions for a human pilot. The outer loop controls the drone position with a PID controller that sends attitude commands to the inner loop. The inner loop then uses the INDI controller. The INDI controller is separated between the outer attitude loop and the inner angular rate loop. The outer loop uses a PD controller that calculates the desired angular rate. The angular rate controller uses the control effectiveness matrix and a first order rotor model to estimate the rotor rate command for each rotor.

The intended goal was to adapt the controller for use in the wind tunnel experiment. The proposed controller needed to be adapted for use in the wind tunnel, as it was only implemented and tuned for manually piloted hover control.

Different tuning was used for each configuration. This stems from the problem that control over yaw is desired only up to varying degrees. In the baseline configuration, the drone is quite capable in controlling yaw. It's body is however asymmetric in the yz-plane and it's elongated nose noticeably counteracts turning the nose towards the flow at very high wind speeds.

With the bumpers attached, this asymmetric force becomes quite difficult to overcome. For example, with the bumpers attached, at higher wind speeds the actuated yawing moment was not enough to overcome counteracting forces. This results in a high command signal to overturn control of other desired states. A higher yaw priority would result in more excitation to overcome the block, at the cost of crashes and altitude control.

The weights assigned to the controller were $W = [1000\ 1000\ 500\ 1]$, according to which the INDI controller prioritizes maintaining pitch and roll, after which thrust is maintained, and yaw commands are only followed if the actuators are not saturated. For the single actuator damage case, $W_{yaw} = 0$, and control was relinquished completely.

F. Input design

Control input during the experiment is designed to achieve as many sets of states as possible. To achieve those possible sets, the vehicle was subjected to a variety of position commands. As the theory of modeling suggested, the most important axis are in the horizontal plane, the vertical plane and yaw rotation.

In order to force the quadrotor to exhibit dynamic behavior and optimize the flight envelope reached, the controllers were tuned to promote aggressive tracking of the control command. By varying the position controller gains and the control sequences, a range of states was covered each flight. Manual flights were performed as well to validate the results and allow for more coverage of the flight envelope.

IV. Data fusion and state estimation

The data gathered from the experiment includes noise and biases. Additionally, not all desired states are directly measured and as such state estimation is applied. There are two sources of information. First, the onboard logger which collected data on the rotors and the accelerations and rotational rate. Second, the OptiTrack positioning system that logged marker positions and provides an estimate of body position and attitude. This section describes the sensor sources, the algorithms used for state, bias and rotor rate estimation.

A. Sensor information

The first source of information comes from the onboard logger. The logger runs on the 512 Hz loop, but the data is not consistently logged at 0.002 ms intervals. Data is logged from the MPU 6050 Inertial Measurement Unit (IMU) sensor and the back-EMF rotor rate sensor.

The IMU is situated around 2 mm to 4 mm in front of the Center of Gravity (C.G.). It's measuring axis are along the axis of the body frame, albeit with a small error. It measures proper acceleration and angular velocity. However, the measurements are heavily influenced by vibrations in the frame. This is evidenced by high noise peaks that can be seen between 80 Hz and 100 Hz. This noise is likely from the imbalances in the rotors, as the noise frequently coincides with the rotor frequency. However, since the frame of the Bebop is split in two parts, the accelerometer only measures the damped vibrations as experienced by the main body part.

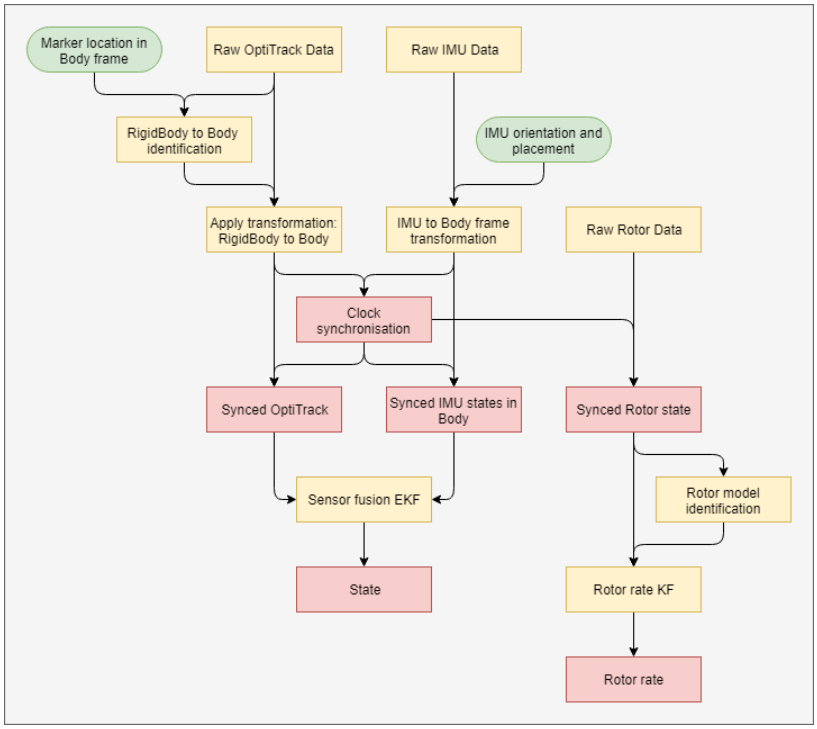

Fig. 3 Schematic of state estimation setup

B. Position and attitude reconstruction

The vehicle position and attitude are measured indirectly. As such they need to be reconstructed from the OptiTrack system. A short overview is given in Section III.D. The available data for reconstruction is stated below. All are logged at the OptiTrack camera frame rate, set at 360 Hz.

- Earth frame marker positions: $\bar{p}_{i,E}$. Usually for 6 or more markers.

- RigidBody position, $\bar{p}_{rb,E}$. This position represents the center of the RigidBody object center, around which the attitude is calculated
- RigidBody orientation $\bar{\phi}_{rb,E}$. The attitude of the RigidBody, as seen from its center. Although this is logged and handled in quaternions, Euler angles are used for readability.

The desired information is the position, attitude and velocity of the actual vehicle in the body frame. In order to achieve this, the transformation from the rigid-body frame to the body frame needs to be known.

$$\bar{p}_{i,R} = T(\bar{\phi}_{rb,E})_E^R \cdot \bar{p}_{i,E} - \bar{p}_{rb,E} \tag{2}$$

The next step is to find the transformation between the marker positions in the Rigidbody frame w.r.t. the Body frame. This is solved using nonlinear least squares solver, as shown in the solver statement in Eq. (3), with the cost function stated in Eq. (4).

$$\min_{x \in S} \|f(x)\|_2^2, \; x = [\bar{\phi}_R^B, \; \bar{p}_{R,B}] \tag{3}$$

$$f(\bar{\phi}_R^B, \bar{p}_{R,B}) = \bar{p}_{i,B} - T(\bar{\phi}_R^B) \cdot \bar{p}_{i,R} - \bar{p}_{R,B} \tag{4}$$

The resulting transformation is then used to correct Rigidbody position and orientation to the body frame.

$$\bar{p}_{b,E} = \bar{p}_{rb,E} - T_E^B \cdot \bar{p}_{R,B} \tag{5}$$

The body velocity of the drone C.G. is then calculated by numerically differentiating the position in the respective frame, using the first order central difference method. It must be noted that this increases noise, but it preferred over directly using position for sensor fusion, as this would complicate the Extended Kalman Filter (EKF).

C. Time series synchronization

The two different sensor setups need to be synchronized before any fusion can be applied. In this case, it was experimented with various methods. Some experimentation was performed with Dynamic Time Warping (DTW), but this resulted in skewed results, due to biases in the signals.

The best approximation was found by using cross correlation of the signals to infer a time delay between when the two logs were started. The found delay was then improved upon by optimizing a cost function for time shift and biases, such that the signals truly match. No significant errors over time were found, but it is still advised to use short flights or divide the data in segments.

D. Bias filtering using Extended Kalman Filter

The forces and moments are indirectly calculated from the inertial sensors. These sensors however contain (vibration) noise and slow time-varying biases. A filter was designed and implemented, based on the filter used by [15].

The EKF relies on predicting the vehicle states based on the IMU measurements. By comparing this with the measurements taken from an reference frame (OptiTrack), the inertial measurements can be corrected.

Equations (6),(7) and (8) form the EKF state space, prediction and innovation equations respectively. The input and output vectors are shown in Eqs. (9) and (11), with the state vector defined by Eq. (10).

The kinematic model forms the basis of the EKF, given in the form: $\dot{x} = f(x, u)$, as it is used to predict the states from the inertial measurements. It is given in Eq. (13). The derivatives of the bias states are assumed 0, i.e. free walking parameters.

$$x(t_{k+1}) = f(x_k, u_k, t_k) + g(u_k, t_k) + w(t_k) \tag{6a}$$
$$z(t_k) = h(x, u, t_k) + v(t_k) \tag{6b}$$

$$\hat{x}(t_{k+1,k}) = \hat{x}_{k,k} + \int_{t_k}^{t_{k+1}} f(\hat{x}_{k,k}, u_k, t) dt \tag{7a}$$
$$P_{k+1,k} = \Phi_{k+1,k} P_{k,k} \Phi_{k+1,k}^T + \Gamma_{k+1,k} Q_{k+1} \Gamma_{k+1,k}^T + Q_b \tag{7b}$$

$$K_{k+1} = P_{k+1,k} H_k^T [H_k P_{k+1,k} H_k^T + R_{k+1}]^{-1} \tag{8a}$$
$$\hat{x}_{k+1,k+1} = \hat{x}(t_{k+1,k}) + K_{k+1}[z_{k+1} - h(\hat{x}_{k+1,k}, u_{k+1})] \tag{8b}$$
$$P_{k+1,k+1} = P_{k+1,k} - K_{k+1} H_k P_{k+1,k}^T \tag{8c}$$

$$\bar{u} = \begin{bmatrix} \bar{\omega}_m & \bar{a}_m \end{bmatrix} \tag{9}$$

$$\bar{x} = \begin{bmatrix} \bar{\phi}_E^B & \bar{v}_B & \bar{\omega}_{bias} & \bar{a}_{bias} \end{bmatrix} \tag{10}$$

$$\bar{z} = \begin{bmatrix} \bar{v}_{B,meas} & \bar{\phi}_{E,meas}^B \end{bmatrix} \tag{11}$$

$$\bar{V}_m = \bar{V}_B + \bar{\epsilon}_V \tag{12a}$$
$$\bar{\phi}_m = \bar{\phi} + \bar{\epsilon}_\phi \tag{12b}$$

$$\dot{\bar{\phi}} = E'_{123}(\psi, \theta, \phi) \cdot (\bar{\omega} - \bar{\omega_b}) \tag{13a}$$
$$\bar{a} = \bar{a}_m - \bar{a}_b + (\bar{\omega} - \bar{\omega_b}) \times \bar{v}_B - T_E^B \cdot \bar{g}_E \tag{13b}$$

The equation for the state covariance matrix P was adjusted, by modifying the system noise matrix.

E. Angular rotor rate state estimation

The direct rotor rate measurement quality is not sufficient to apply central difference differentiation. A linear Kalman filter is introduced, based on a first order delay, see Eq. (14). The parameters of the model are found by least squares.

$$\dot{\omega} = \tau^{-1}(\omega_u - \omega_z) \tag{14}$$

The input to the Kalman Filter (KF) is the commanded angular rate signal. Although this signal is by definition known, as it is sent by the autopilot, it is also discrete and as such the input noise matrix value is based on the discrete time step. The measurement signal is based on the back-EMF measurement. Since numerical differentiation is unfeasible on this discrete signal, there is no observation to be made with regards to the rotor rotational acceleration, as was done with the numerical differentiation of the position, measured by OptiTrack, to velocity.

V. Results

This section presents the results gathered from the experiment. Firstly the vehicle properties are determined, mainly the inertia tensor. Secondly the covered flight envelope is shown. Then an overview of the quality of the EKF state estimates is given. Fourthly results from the rotor state KF are shown and lastly in depth analysis of the measurement data is conducted , with respect to the input design.

A. Vehicle inertial properties

The procedure for estimating the vehicle inertia follows [16]. The vehicle is dissembled into its individual parts and by measuring their properties the inertia is calculated using the parallel axis theorem.

To determine the inertia matrix of the vehicle, the vehicle was dissembled into its individual parts. Parts were weighed and their c.g.'s and approximate dimensions measured. The total vehicle inertia was calculated by assuming simplified shapes to represent individual parts. This method was verified in [16] to be relatively accurate ($\epsilon < 5$ %) for a similar vehicle.

Table 2 Moment of inertia and rotational tensor values for the Parrot Bebop 1.

Configuration	Mass$[kg]$	I_xx$[kg \cdot m^2]$	I_yy $[kg \cdot m^2]$	I_zz $[kg \cdot m^2]$	I_xz$[kg \cdot m^2]$
Standard	.3880	.001077	.001132	.002074	.000011
Two bumpers	.4122	.001820	.001354	.003034	.000011
Right bumper	.4001	.001438	.001243	.002543	.000011
All actuators damaged	.3880	.001073	.001127	.002065	.000011
Actuator 0 damaged	.3880	.001075	.001130	.002069	.000011

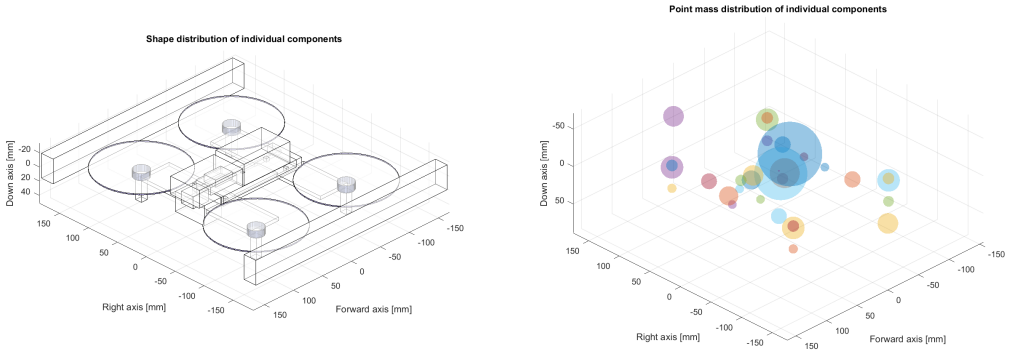

(a) Assumed shape of each individual component. **(b) Relative mass of each individual component.**

Fig. 4 The moment of inertia is estimated from the individual components. These schematics show the data used for a dual bumper configuration.

B. Flight envelope

In Figs.5,6, and 7, the resulting envelopes are shown for all configurations. For the bare configuration in Fig. 5a, the resulting flight envelope covers body velocities up to $15\,\mathrm{m\,s^{-1}}$. The maximum descend velocity is significantly lower, due to the small test section preventing large excitation in vertical direction. No other significant gaps are detected. The circular effect is mainly due to the rotations performed at higher wind tunnel speeds. An improvement would be to couple lateral and vertical movement to fill the flight envelope ceiling. The body rotational rates are seen to reach about $10\,\mathrm{rad/sec}$ for each axis. Coupled data remains sparse, due to the lack of yawing motions incorporated during position excitations.

The addition of the two bumpers significantly reduces the flight envelope, see Figs. 6a & 7a. Due to the added drag, the Bebop had difficulty maintaining stability at speeds beyond $10\,\mathrm{m\,s^{-1}}$. Also command of yaw at higher rates showed interesting behavior. Due to the backwards inwards-folding shape of the bumpers, aerodynamic forces induced a steering effect. The quadrotor sometimes was required to start at a desired angle, or it could otherwise not reach it. Pitch and roll rates appear unaffected.

This behavior is even more prevalent with a single bumper. In Fig. 7b it can be seen that this configuration was able to achieve higher yawing rates ($15\,\mathrm{rad\,s^{-1}}$) then with two bumpers. This was most likely caused by the extra bumper causing a rudder effect and exciting the quadrotor to higher rates. Due to this steering, a visible asymmetry is present in the velocity envelope in Fig. 6b.

The flight envelope of the four actuators damaged configuration (Fig. 6c & 7c) shows a resemblance to the baseline

flight envelope in Fig. 5. However, all limits are reduced to about $10\,\mathrm{m\,s^{-1}}$ or $7\,\mathrm{rad\,s^{-1}}$. Since no significantly destabilizing factors were present, the drone was able to function in most conditions, but was limited by the required thrust to overcome higher wind speeds.

The envelope of a single actuator damaged, see Figs. 6d & 7d, shows the most significant difference. Unable to maintain heading, the velocity envelope becomes effectively two dimensional. Climb speeds were significantly reduced, as well as descend without crashing. The yaw rate is at a constant 10 to $15\,\mathrm{rad\,s^{-1}}$. Maximum pitch and roll rates are reduced slightly, but are actively engaged in order to maintain stability.

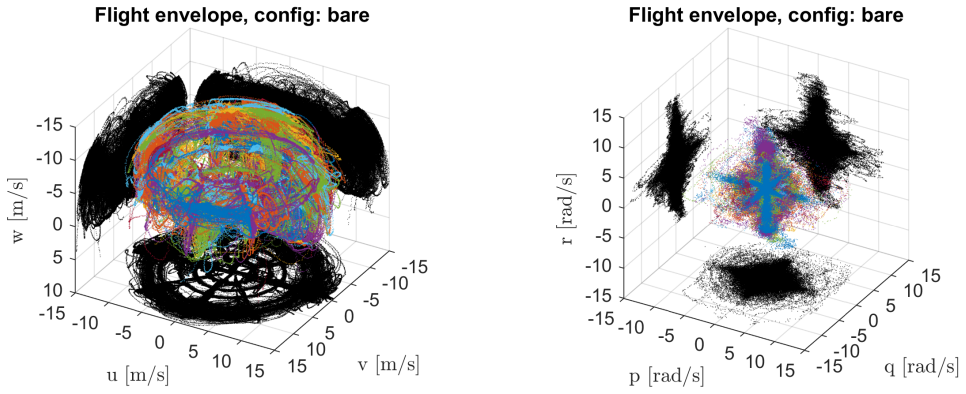

(a) $\bar{V}$ **(b)** $\bar{\Omega}$

Fig. 5 The flight envelope for the bare configuration. On the left: expressed in the body velocities, with respect to the airflow. On the right: body rotational rates. Colours indicate different flights used to gather the dataset. The flight envelope contours are expressed as the projections in black.

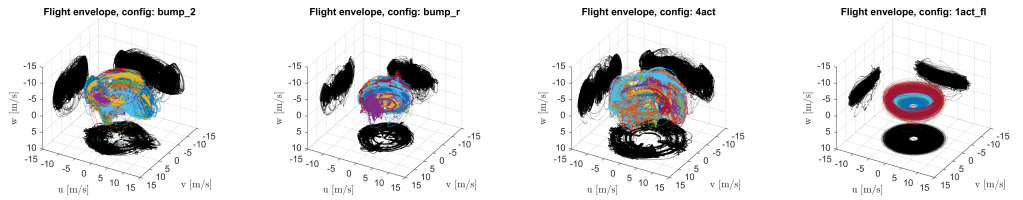

(a) Two bumpers **(b) Right bumper** **(c) All actuators damaged** **(d) Single actuator damaged**

Fig. 6 The flight envelopes expressed for four configurations. Flight envelope expressed in body velocities, with respect to the airflow. Colours indicate different flights used to gather the dataset. The flight envelope contours are expressed as the projections in black.

C. Bias estimation of EKF

Figure 8 shows the estimated bias for a single flight. As can be seen, the gyroscope biases are much more constant than the specific force biases. Both biases show quick convergence to their final std. dev. estimates in Fig. 9. The steady state term was added to allow some free walk on the biases. This was necessary to track the variable, when certain conditions changed, such as a heading change. This indicates two things. The bias is tracking something else then the slow time varying bias, and that is dependent on orientation. A notable lack in this experiment has been the calibration of the IMU orientation, with respect to the body, between flights. Although rigidly attached to the board, the optitrack rigid body frame is not. This could influence these measurements, and is highly recommended for future research. Another phenomena, not shown here, was a drop in standard deviation estimate for f_b, correlationg with landing and subsequent decrease in vibrations.

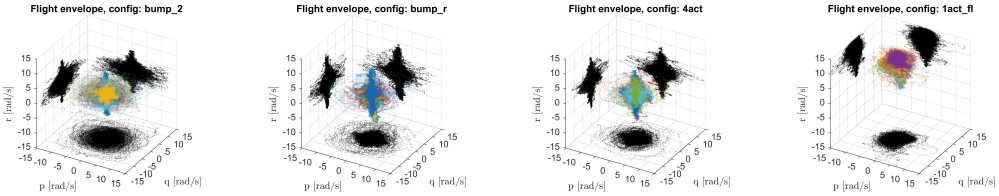

(a) Two bumpers **(b) Right bumper** **(c) All actuators damaged** **(d) Single actuator damaged**

Fig. 7 The flight envelopes expressed for four configurations. Flight envelope expressed in body rotational rates. Colours indicate different flights used to gather the dataset. The flight envelope contours are expressed as the projections in black.

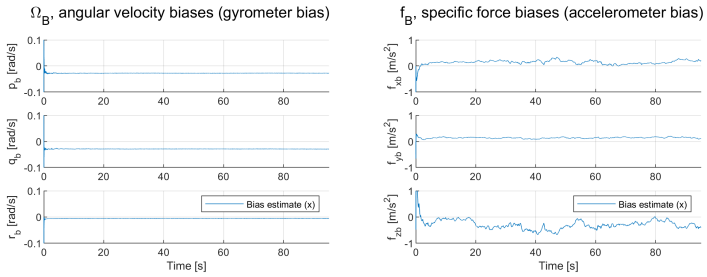

(a) Rotational velocity bias **(b) Specific force bias**

Fig. 8 IMU bias estimates for Flight 20.

D. Improvements in rotor state estimation

Figure 10a shows the raw angular rate command and observation, together with its KF estimate. Figure 10b shows the angular acceleration of the rotors estimated by central difference, together with the KF estimate. Clearly the KF produces a smoother angular acceleration estimate. The main reason is the limited resolution of the measurement causing a increase in noise on the angular acceleration estimate, which is now reduced by the first order model used by the KF. The time constant of that model was consistently estimated at $\tau = 0.049$ for multiple dozens of flight tests.

E. System identification inputs

The five types of excitations are longitudinal flight, lateral flight, yawing motions, heaving (climbing and descending) and manual pilot commands. In Fig. 11 the resulting flight path for each type of input is shown. This is the result of the quadrotor following a set of waypoints, with an aggressively tuned position controller. The exception is yaw, where the inputs are generated by changing desired heading command. The yawing input type consists solely of heading changes, but for each of the other input types, the heading was changed as well, between each sequence. Figs. 11-16 show the results for each of these sequences. They are the combination of two flights, performed at $5\,\mathrm{m\,s^{-1}}$ in the baseline configuration.

The longitudinal excitation is designed to look at the pitch and roll rates at various velocities. It is the main flight mode for the quad rotor in normal circumstances. The resulting states are shown in Fig. 12. The excitation can be seen in the earth position's North component. Here it first moves backwards, before moving into the wind. Since in this case the nose is pointing East, the roll angle mostly excited during the direction changes. Large peaks in thrust command can be seen in Fig. 12g, around 155 seconds, where it is both climbing and moving into the flow.

The lateral excitation is designed similarly to the longitudinal mode. However since it is now effectively flying sideways, new commands do not require the amount of extra thrust to overcome the flow to reach a new position as with the longitudinal mode. Figure 13 shows the resulting states have good excitation in the pitch and roll angles, as well as Ω and the respective Moment vector.

The heaving mode in Fig. 14 is designed to excite the thrust dynamics by experiencing both positive and negative

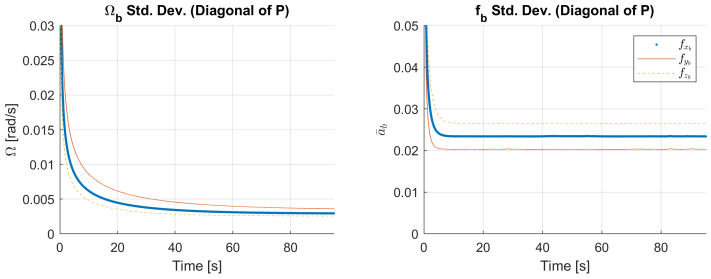

(a) Rotational velocity bias std. dev **(b) Specific force bias std. dev.**

Fig. 9 IMU bias standard deviation estimates for Flight 020.

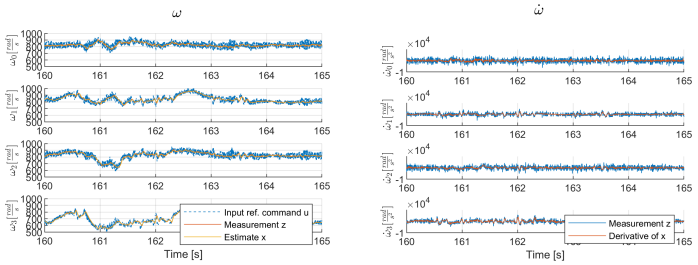

(a) Rotor rates for each actuator. The blue lines indicates the given command, which fluctuates significantly due to the controller.

(b) Rotor acceleration for each actuator. The blue line indicates the direct differentiation. The red line displays the KF estimate.

Fig. 10 Rotor states.

wind velocity in the z-direction. This way the intake of each rotor experiences a varying range of velocities, and thrust efficiency as expected by quadrotor models. The climbing and descend velocities are gradually increased, up to the point that is allowed by the test section. The resulting states show good excitation in thrust and force. Note that the rotational dynamics still show some excitation, that the controller counteracts, resulting in the varying moment vector.

The yawing mode was added to investigate the responsiveness to yaw commands. This mode is essential for steering, but is also very important for loss of controls scenarios, where the drag in yaw is expected to stabilize the motion. The result to a sequence of heading changes is shown in Fig. 15. Here the variation of forces and moments can most clearly be seen, as a change in heading also means a new equilibrium. This is not clearly seen in the previous Figures, as they only shown the sequences for one heading.

The last mode flown for each configuration was a manual made, for which an example is shown in Fig. 16. In this mode, a human pilot manually controls the reference position, allowing for stable, but more aggressive flights. Special care was taken to excite pitch and roll at similar times, in order to maximize the amount of coupled states that were flown.

VI. Conclusion

In this paper, a methodology is presented to facilitate free-flight system identification for quadrotor dynamics. The methodology is suited for a compromised quadrotor, in high-speed conditions. The methodology was tested for five configurations. A baseline off-the-shelf quadrotor is given first. The baseline is then modified with two bumper attachments, and subsequently one is removed. The last two configurations are tested with one or two effectiveness reduced actuators.

For the methodology to work, a suitable fault-tolerant controller was selected, the Incremental Nonlinear Dynamic

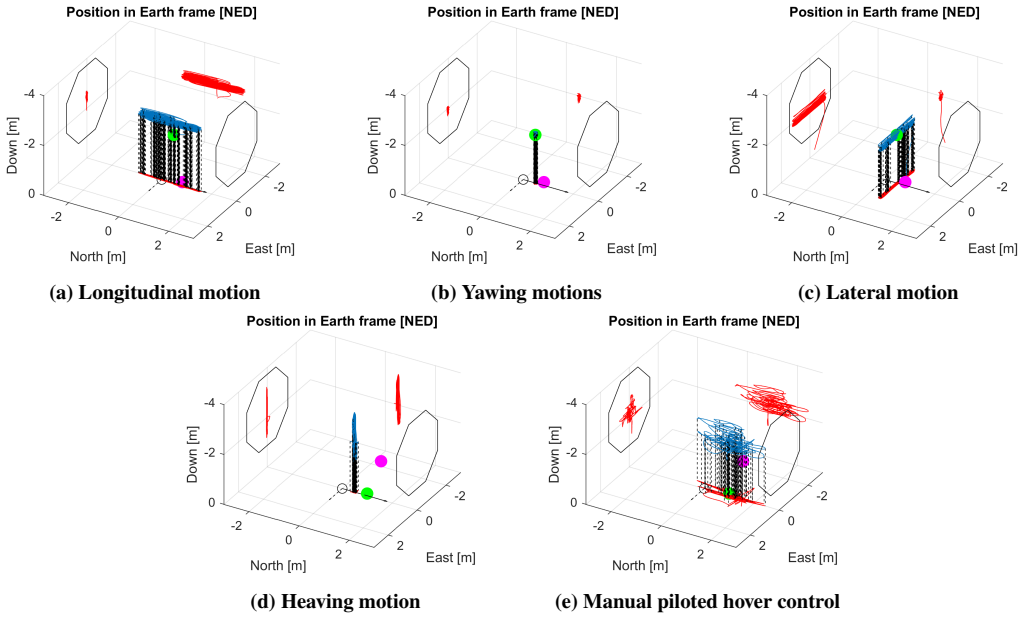

(a) Longitudinal motion **(b) Yawing motions** **(c) Lateral motion**

(d) Heaving motion **(e) Manual piloted hover control**

Fig. 11 Flight path for each input type.

Inversion (INDI) controller, with Weighted Least Squares (WLS) priority optimized control allocation. This combination proved very effective to fly the compromised quadrotor in off-nominal conditions, even with full loss of control in yaw.

Careful selection was made with regards to the system inputs during the experiment, in order to excite as many combinations of states. The results of this show the desirable states to be sufficiently excited, It is however left up to future research to identify models using this dataset.

In order to improve the quality of the data gathered, a sensor fusion algorthim was implemented, utilizing a Extended Kalman Filter (EKF) based on a kinemeatic model relating the external observer based motion tracking data with the onboard Inertial Measurement Unit (IMU) data. With these sensors, the goal to derive a suitable Forces & Moments (F&M) dataset, related to the system input $\bar{\omega}$ was satisfied. Through tuning, steady state filtering of the biases and reorganizing, the filter was able to cope with the vibrations as well as the IMU biases. The calibration process is shown to be incomplete, but otherwise the F&M can be estimated reliably.

Care must be taken to verify and validate the rigid body assumption. For the Parrot Bebop v1 this is tested through the addition of the bumpers as well as the dampers in the structure. The higher sensor rate of the OptiTrack measurements compared to earlier research has aided in increasing the certainty of the acceleration data.

Time synchronization is a tricky subject, especially on small time scales. It is advised that advantage is taken in the future of the GPS clock to determine clock errors. This could allow for more dynamics to be modelled for individual rotor rotations. The author recommends that OptiTrack logging start and stop signals are sent to the drone. This is possible according to the OptiTrack API documentation. The data can be corrected for latency and the onboard logger can be programmed to synchronize with the OptiTrack logger function.

A more precise marking system can aid in the calibration between the two data sources. Future research should also aim to add additional IMU sensors on the multiple bodies in cases such as with the Bebop v1 and v2.

Appendix

Acknowledgments

The authors would like to thank and acknowledge the following people.

For granting access and support for and during the wind tunnel experiment: Nando Timmer. For his invaluable

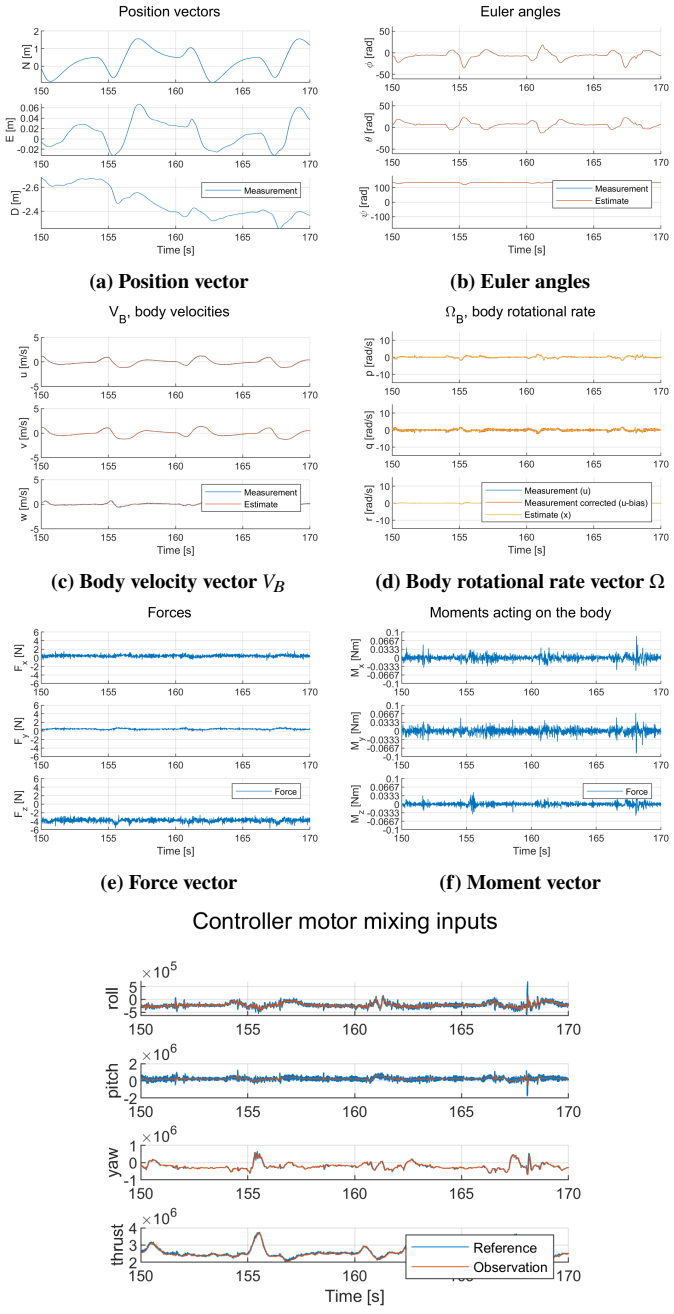

(a) Position vector **(b) Euler angles**

(c) Body velocity vector V_B **(d) Body rotational rate vector Ω**

(e) Force vector **(f) Moment vector**

(g) Motor mixing inputs. Each index represents the imbalance created by the rotor to control the respective state.

Fig. 12 Resulting states from a longitudinal excitation, performed at $5\,\mathrm{m\,s^{-1}}$ in the baseline configuration. .

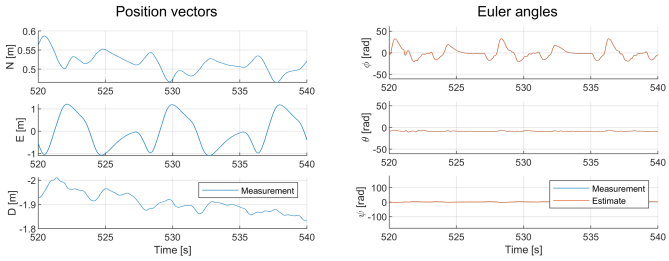

(a) Position vector

(b) Euler angles

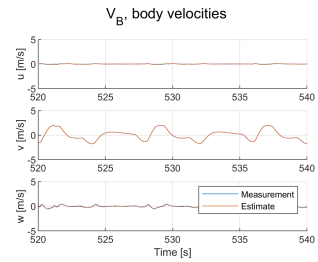

(c) Body velocity vector V_B

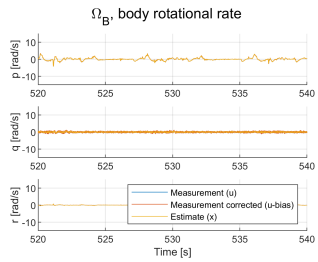

(d) Body rotational rate vector Ω

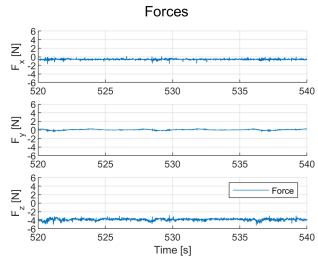

(e) Force vector

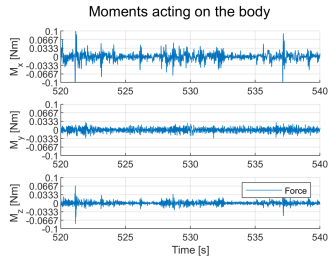

(f) Moment vector

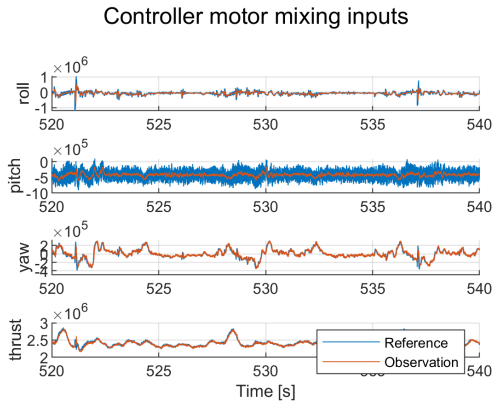

(g) Motor mixing inputs. Each index represents the imbalance created by the rotor to control the respective state.

Fig. 13 Resulting states from a lateral excitation, performed at $5\,\mathrm{m\,s^{-1}}$ in the baseline configuration.

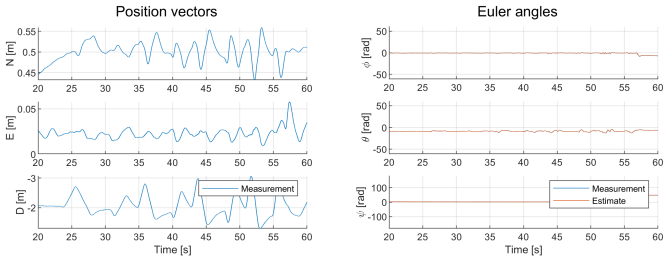

(a) Position vector

(b) Euler angles

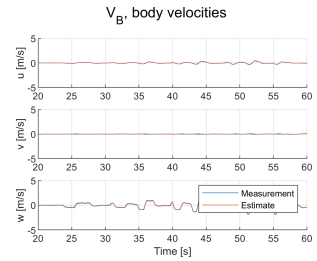

(c) Body velocity vector V_B

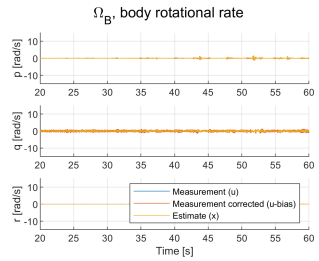

(d) Body rotational rate vector Ω

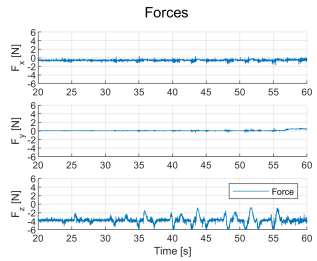

(e) Force vector

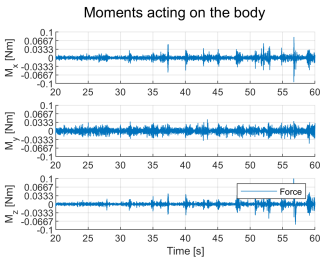

(f) Moment vector

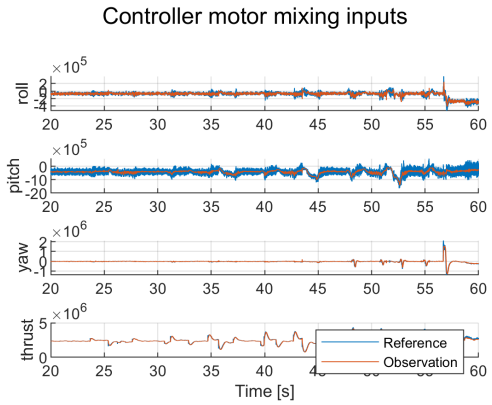

(g) Motor mixing inputs. Each index represents the imbalance created by the rotor to control the respective state.

Fig. 14 Resulting states from a heaving (climbing and descend) excitation, performed at $5\,\mathrm{m\,s^{-1}}$ in the baseline configuration.

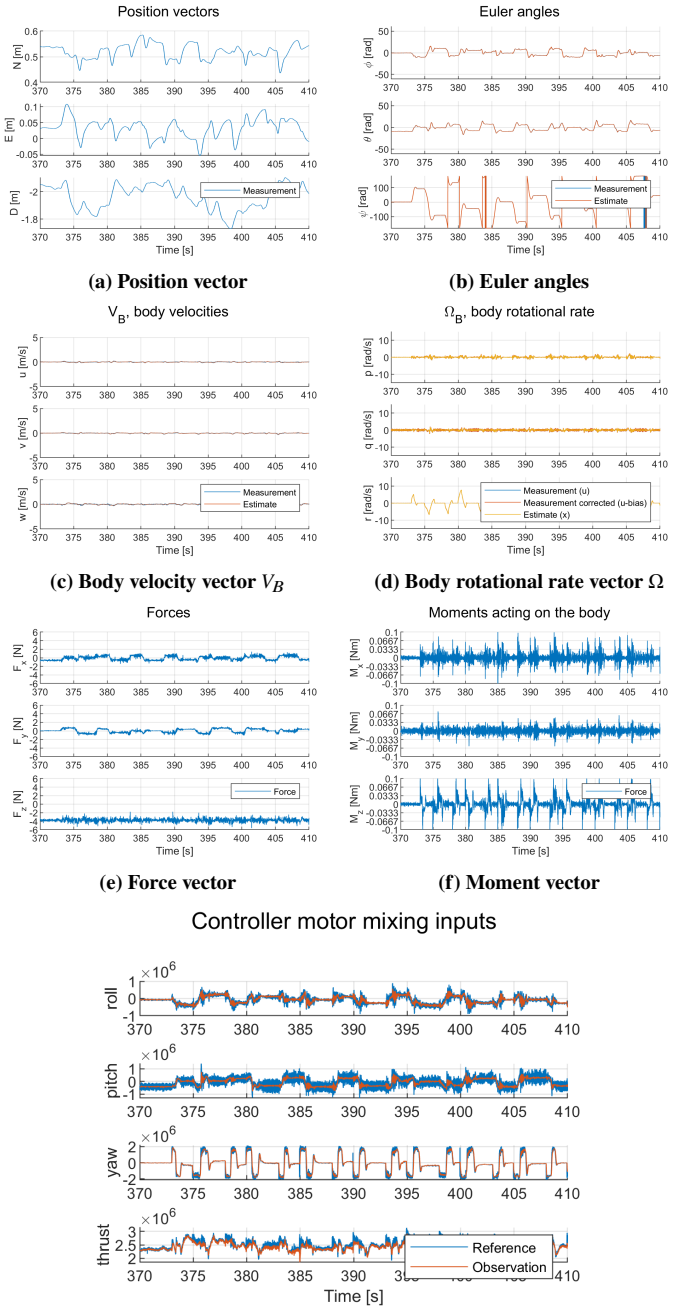

(a) Position vector **(b) Euler angles**

(c) Body velocity vector V_B **(d) Body rotational rate vector Ω**

(e) Force vector **(f) Moment vector**

(g) Motor mixing inputs. Each index represents the imbalance created by the rotor to control the respective state.

Fig. 15 Resulting states from a yawing excitation, performed at $5\,\mathrm{m\,s^{-1}}$ in the baseline configuration.

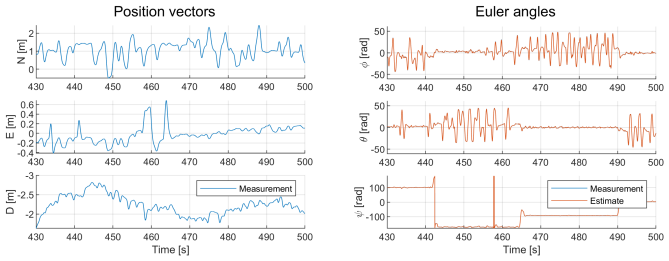

(a) Position vector

(b) Euler angles

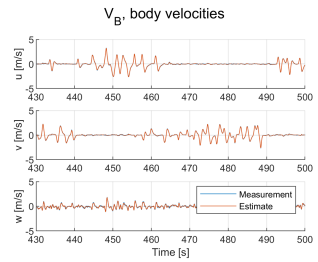

(c) Body velocity vector V_B

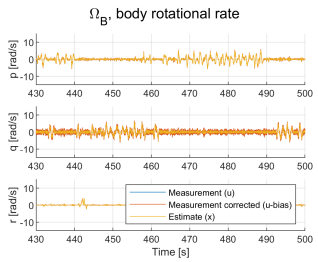

(d) Body rotational rate vector Ω

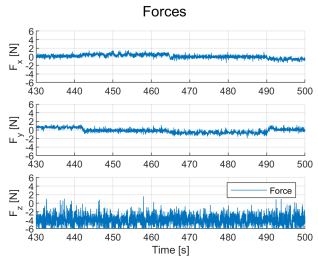

(e) Force vector

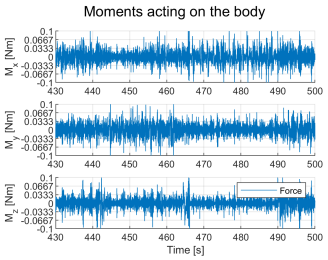

(f) Moment vector

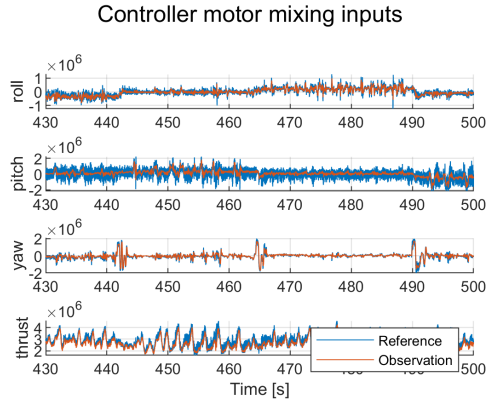

(g) Motor mixing inputs. Each index represents the imbalance created by the rotor to control the respective state.

Fig. 16 Resulting states from a manual excitation, performed at $5\,\mathrm{m\,s^{-1}}$ in the baseline configuration.

knowledge on the bebop systems, paparazzi code and OptiTrack system: Erik van der Horst. For his support in setting up the windtunnel experiment and knowledge of previous experiments: Matej Karasek. For his research on the INDI controller and continued support on paparazzi code implementations and adaptations: Ewoud Smeur. For providing the basis of the EKF code and information on her set-up: Sofie Armanini.

References

[1] Norouzi Ghazbi, S., Aghli, Y., Alimohammadi, M., and Akbari, A. A., "Quadrotors unmanned aerial vehicles: A review," *International Journal on Smart Sensing and Intelligent Systems*, Vol. 9, No. 1, 2016, pp. 309–333.

[2] Hoffmann, G. M., Huang, H., Waslander, S., and Tomlin, C. J., "Precision flight control for a multi-vehicle quadrotor helicopter testbed," *Control Engineering Practice*, Vol. 19, No. 9, 2011, pp. 1023–1036. doi:10.1016/j.conengprac.2011.04.005, URL https://www.scopus.com/inward/record.uri?eid=2-s2.0-79960891417&partnerID=40&md5=1ece5efa1742135b0b47f287f69099a9http://linkinghub.elsevier.com/retrieve/pii/S0967066111000712.

[3] Powers, C., Mellinger, D., Kushleyev, A., Kothmann, B., and Kumar, V., "Influence of Aerodynamics and Proximity Effects in Quadrotor Flight," *Springer Tracts in Advanced Robotics - Experimental Robotics*, Vol. 88, Springer, 2013, pp. 289–302. doi:10.1007/978-3-319-00065-7, URL http://link.springer.com/chapter/10.1007/978-3-319-00065-7_21.

[4] Huang, H., Hoffmann, G. M., Waslander, S. L., and Tomlin, C. J., "Aerodynamics and control of autonomous quadrotor helicopters in aggressive maneuvering," *2009 IEEE International Conference on Robotics and Automation*, IEEE, IEEE, 2009, pp. 3277–3282. doi:10.1109/ROBOT.2009.5152561, URL http://ieeexplore.ieee.org/document/5152561/.

[5] Mahony, R., Kumar, V., and Corke, P., "Multirotor aerial vehicles: Modeling, estimation, and control of quadrotor," *IEEE Robotics and Automation Magazine*, Vol. 19, No. 3, 2012, pp. 20–32. doi:10.1109/MRA.2012.2206474.

[6] Bristeau, P.-J., Martin, P., Salaün, E., and Petit, N., "The role of propeller aerodynamics in the model of a quadrotor UAV," *European Control Conference Proceedings*, IEEE, IEEE, 2009, pp. 683–688. URL http://cas.ensmp.fr/~petit/papers/ecc09/PJB.pdf.

[7] Zhang, X., Li, X., Wang, K., and Lu, Y., "A Survey of Modelling and Identification of Quadrotor Robot," *Abstract and Applied Analysis*, Vol. 2014, 2014, pp. 1–16. doi:10.1155/2014/320526, URL http://www.hindawi.com/journals/aaa/2014/320526/.

[8] Foster, J., and Hartman, D., "High-fidelity multirotor unmanned aircraft system simulation development for trajectory prediction under off-nominal flight dynamics," *17th AIAA Aviation Technology, Integration, and Operations Conference, 2017*, 2017.

[9] Sun, S., Schilder, R., and de Visser, C. C., "Identification of Quadrotor Aerodynamic Model from High Speed Flight Data," *2018 AIAA Atmospheric Flight Mechanics Conference*, American Institute of Aeronautics and Astronautics, Reston, Virginia, 2018. doi:10.2514/6.2018-0523, URL https://arc.aiaa.org/doi/10.2514/6.2018-0523.

[10] "Paparazzi Wiki," , ???? URL https://wiki.paparazziuav.org/wiki/Main_Page.

[11] Lignarolo, L., Ragni, D., Krishnaswami, C., Chen, Q., Simão Ferreira, C., and van Bussel, G., "Experimental analysis of the wake of a horizontal-axis wind-turbine model," *Renewable Energy*, Vol. 70, 2014, pp. 31–46. doi:10.1016/j.renene.2014.01.020, URL http://flow-offshore.nl/images/flow-openbaar/p201101_012_tud_bijlage.vi.progress.report.h1.2014_v01.pdfhttp://linkinghub.elsevier.com/retrieve/pii/S0960148114000494.

[12] Smeur, E., Chu, Q., and De Croon, G., "Adaptive incremental nonlinear dynamic inversion for attitude control of micro air vehicles," *Journal of Guidance, Control, and Dynamics*, Vol. 39, No. 3, 2016. doi:10.2514/1.G001490.

[13] Hoppener, D., "Actuator Saturation Handling using Weighted Optimal Control Allocation Applied to an INDI Controlled Quadcopter," Ph.D. thesis, 2016.

[14] Smeur, E. J. J., de Croon, G. C. H. E., and Chu, Q., "Cascaded Incremental Nonlinear Dynamic Inversion Control for MAV Disturbance Rejection," , No. February, 2017. URL http://arxiv.org/abs/1701.07254.

[15] Armanini, S. F., Karásek, M., de Croon, G. C. H. E., and de Visser, C. C., "Onboard/Offboard Sensor Fusion for High-Fidelity Flapping-Wing Robot Flight Data," *Journal of Guidance, Control, and Dynamics*, 2017, pp. 1–12. doi:10.2514/1.G002527, URL https://arc.aiaa.org/doi/10.2514/1.G002527.

[16] Mendes, A., van Kampen, E., Remes, B., and Chu, Q. P., "Determining moments of inertia of small UAVs: A comparative analysis of an experimental method versus theoretical approaches," *AIAA Guidance, Navigation, and Control Conference*, American Institute of Aeronautics and Astronautics, Reston, Virigina, 2012, pp. 1–14. doi:10.2514/6.2012-4463, URL http://arc.aiaa.org/doi/10.2514/6.2012-4463.

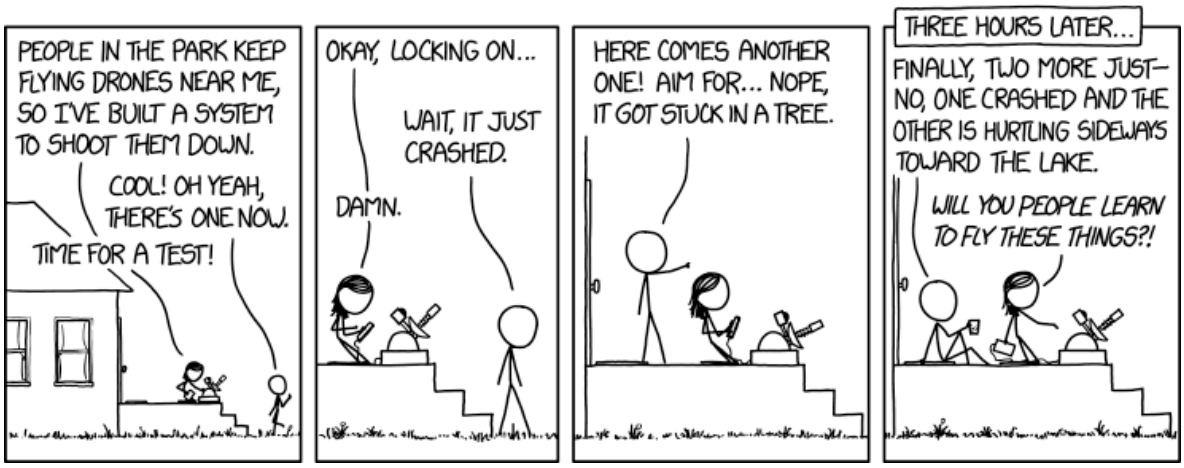

Figure 1: "Drone Problems" by Randall Munroe; xkcd.com/1846/

Chapter 1

Introduction

Multirotor drones are becoming more and more popular with new applications emerging virtually every day. Small personal drones such as quadcopters will soon be an everyday occurrence. With a growing interest and usage due to their wide range of applications, incidents are more likely to occur and significant improvements in drone safety become a necessity.

With all these new additions to the airspace, requirements for drones will become stricter, especially if the tasks required are performed in urban environments. Drones will be expected to perform safely and accurately in high-end conditions. These include not only aggressive manoeuvres, high-speed winds, and turbulence, but also resistance to damage due to any source. As such, when looking to the future, it is deemed vital to investigate drones under high speed and compromised circumstances, see for example Norouzi Ghazbi, Aghli, Alimohammadi, and Akbari (2016).

This chapter introduces the background of the selected topic, stating the project aims and accompanying research questions that the project intends to answer. The last section then is intended as a guide to the rest of this preliminary thesis, giving an overview of the covered topics.

1-1 Background

Within the past few years, non-violent drones have seen a rapid rise in their usage. In the near future, the market is expected to increase even further. Reported estimates include a 100-billion-dollar market for unmanned aerial vehicles (UAV), including military use, in 5 years with 20 billion dollars in commercial and consumer markets, see Mills (2016). Past year alone in America, 400.000 vehicles were registered as part of a new set of regulations.

With respect to outdoor environments, drones are intended for delivery, reconnaissance, infrastructures inspection and more. These drones will frequently be operating in a high-speed flight conditions, while facing non-negligible aerodynamic effects.

One significant challenge with current drones is their fault tolerance. Currently, most research into fault-tolerant controllers is diverted to actuator effectiveness, which often neglects the complicated nonlinear and coupled effects a structural damage event can cause. If such a failure occurs, a crash is almost always unavoidable. Improved fault tolerant controllers must be created to prevent such a drone from exciting its safe flight envelope, and hence allow it to land.

Estimation of flight envelopes is currently done by applying reachability analysis, see Mitchell, Bayen, and Tomlin (2005), utilizing high fidelity models to determine the bounds beyond a vehicle should not go, or risk becoming uncontrollable. Research is also being done to make these methods available for on-line estimation by Stapel, de Visser, Van Kampen, and Chu (2016).

Modelling the effects of a damage event requires methods to identify and validate. Current methods for general aviation include computer analysis or expensive and dangerous flight tests near the edge of the flight envelope, see Shah, Foster, and Cunningham (2010). This problem can be avoided with cheap quadrotors. With the allowance of more risk at the boundaries of the flight envelope, safe flight envelope estimators can be validated more thoroughly.

In order to investigate the flight dynamics of the drone and the effects of damage, it is required to fly while subject to damage. With system identification techniques the corresponding models can be identified and compared to baseline models. An experimental setup is to be developed to achieve this in a controlled way.

This research is performed parallel to the implementation of a structural damage case database approach in the general aviation that is envisioned at the Technical University of Delft (TUDelft) by Y. Zhang, de Visser, and Chu (2016). Hence the ultimate product is expected to aid in research of general aviation safety as well.

1-2 Research aim and objectives

1-2-1 Research goal

The goal is to investigate the effect of structural damage to an off-the-shelf quadrotor, in this specific case the Parrot Bebop. The envisioned results are high fidelity models of both the baseline quadrotor and a flyable damaged version, identified using flight data and modern system identification techniques.

The goal is a result of both the consensus that a lack of literature exists on the specific topic, as well as quadrotors being a suitable test platform to experiment with the techniques used for Loss-of-Control research in aircraft. This requires high fidelity models for baseline and damaged aircraft. System identification is a unique way to find these types of models and is as a field still progressing.

1-2-2 Research question and subquestions

The envisioned results are high fidelity models of both the baseline quadrotor and a flyable damaged version, identified using flight data and modern system identification techniques.

The model should give an accurate depiction of the forces and moments encountered during flight. Preferably this model is a globally valid model. This can be more easily compared to other cases with the drone suffering unfavourable conditions.

As such a regressor dependent model appears to be the way to go. From literature, as will be shown in following chapters, it is evident that information is lacking on the higher order dynamics when experiencing faster airspeeds. Damage modelling has been done to the extent of either losing an actuator or assuming a control effectiveness where the lift generated from a single actuator is reduced linearly.

Identification of the models found are also derived from either static wind tunnel tests with a mounted quadrotor, use identification techniques in hover or slow flights or use inaccurate GPS sensors. A significant improvement on this would be to allow the identification of the new model to be derived from actual flight data in a wind tunnel. Here the use of accurate sensors and wind speed control could result in a superior dataset to identify the dynamics in new regions of the flight envelope.

The gap to be answered here is thus framed by the main research question, stated as followed.

How can the Parrot Bebop quadrotor dynamics be modelled for high speed and single actuator loss conditions and identified from a free-flight wind tunnel experiment using modern system identification techniques?

To answer this question, the task is divided into smaller questions which answered together can be used to fill the identified gap.

1. What types of structural damage can affect an off-the-shelf quadrotor?
   (a) What priority do the different types of damage have?
   (b) What changes in dynamic behaviour can be expected from the selected damage cases?
2. What are possible and suitable physical models of the quadrotor to best describe and predict its behaviour to control inputs?
   (a) What (aerodynamic) effects have a significant impact on the forces and moments?
   (b) How can these effects be parametrically modelled?
   (c) How should the system input and output be defined?
3. Which system identification techniques are best suited to identify the model of an off-the-shelf quadrotor, taking into account the selected model structure?
   (a) What suitable types of system identification techniques are available?
   (b) How can the state-of-the-art models of physical effects be incorporated into the identification method and model structure selection?
   (c) How can the quality of the model parameters be assessed?
   (d) What criteria are suitable to assess the quality of the model structure?
   (e) How will the performance of the identification method be compared to established models?

4. How will the chosen model structure, system identification techniques and damage cases be used in a test setup to determine the desired models?
   (a) What inputs are required to excite the quadrotor in order for its dynamics to be accurately determined?
   (b) How can a controller be implemented to allow the drone to fly in the selected flight region and under compromised circumstances?
   (c) What possible challenges pose the selected hardware for the test setup?
   (d) How can external disturbances be recreated?
   (e) How should the information from sensors be used to gather an improved estimate of the data?

1-2-3 Motivation & Feasibility

The first question should be answered by performing an investigation on the most suitable cases to be investigated for this research. The answer will allow for an important damage case to be selected and be informed on the possible effects this will have on any future model. The second question is to be answered from literature and the current state-of-the-art to allow any chosen identification method and chosen model structure to allow for this information to be incorporated and used as comparison.
The third question is the most important one. The identification of the dynamics can be performed in multiple ways and a choice must be mode. Any chosen method should allow comparison with established models from literature. Model structure selection is very important and the quality of the result will depend on the balance between model size and accuracy.
The fourth question is concerned with finding a suitable test setup that will allow enough information to be present in the data. This is essential for proper system identification. As such a controller needs to be chosen that can keep the quadrotor stable in the outer edges of the flight envelope. The drone will have to be excited with various control inputs in order to improve the validity of any identified model over large regions of the flight envelope. Sensor data will also need to be filtered and used to complete the data set.

In order to answer the questions, multiple subgoals can be defined that if all achieved will allow for the answer to present itself.

1. Design a measurement setup that will allow the states to be estimated.
2. Implement a suitable controller for the free-flight experiment.
3. Setup and conduct a free-flight wind tunnel experiment.
4. Implement a state estimation filter that combines information of the dynamics and sensor characteristics to create a true state estimate.
5. Conduct a model structure estimator analysis to identify the important dependent variables.
6. Derive a set of evaluation criteria to validate the identified model structure and its parameters.

Answering these goals requires planning. The time allowed is nine months but is stretched due to the experiment planning and time required to conduct the analysis. Although multiple

cases can and will be tested, the focus will be on a to be determined select few. Other cases will be left for future work and colleagues.

1-3 Content overview

The following chapters discuss the literature and chosen methodologies as they were to be applied in the paper. Chapters 2 to 5 establish the state-of-the-art as it was known. Chapter 2 focuses on the quadrotor modeling techniques used by the community to analyze and predict quadrotor behavior. Chapter 3 establishes known techniques to fuse sensor data to achieve higher precision. The Extended Kalman Filter (EKF) is introduced here, which in turn is used to combine observer data with onboard data, such that biases are mitigated. Chapter 4 details some of the system identification approaches that were found with respect to quadrotor identification. Chapter 5 then closes off the state-of-the-art review with the available controllers that could be suited to control damaged quadrotors.

Chapter 6 details the chosen techniques to be applied for the experiment, with the experiment design and execution detailed in Chapter 7. Some closing remarks are made in the Conclusions.

Chapter 2

Quadrotor modelling

Presented here is the state-of-the-art in quadrotor modelling. This is vital for the selection of appropriate model structures and understanding where a lack of model fidelity is or can be present. These models range from simplistic to extensive physical interpretations of quadrotor aerodynamics.

The research into quadrotor modelling is done up to varying degrees. Multiple university research groups and projects have already invested in these agile vehicles. Among these are the STARMAC I and II project by G. Hoffmann et al. (2004) and by G. M. Hoffmann, Huang, Waslander, and Tomlin (2011) respectively, or the Draganflyer modelled by McKerrow (2004). Models for these drones and other quadrotors have been made up to varying degrees of fidelity, taking into account different effects, such as blade flapping or induced airspeed. The models also differ in how the data was gathered to determine the parameters of each model, such as static experiments as well as free flight data. Interestingly most of these models include those from specifically designed vehicles, where this project uses an off-the-shelf vehicle with the accompanying constraints.

This chapter divides the models into four levels of fidelity, sequentially increasing. The first level entails rigid body dynamics and standard Newtonian models and accompanying assumptions as normally used on quadrotors. Secondly, the main control factors are discussed, which includes nominal thrust and moment provided by the rotors, as well as gyroscopic and reaction moments. The third section presents the predominant aerodynamic effects, that according to literature contribute heavily to model fidelity. The fourth section is concerned with the remaining aerodynamic effects. This focuses on the residual, the forces due to body and rotor or rotor to rotor interactions, aggressive rotational aerodynamics and off-nominal conditions present, for example, damage. The fifth and last section provides a synthesis of the models found and a discussion there-off.

2-1 Equations of motion for a rigid body quadrotor

The basis of any model in quadrotor research is usually a rigid body, with a mass and inertia properties, undergoing a set of forces, as a function of the actuators and vehicle states. As described by Mahony, Kumar, and Corke (2012), the basis of these models is given as in Equation 2-1. These relate the translational and rotational velocities and accelerations to the externally applied forces and moments and the body's mass.

$$\begin{aligned} W \cdot \bar{g}_b + \bar{F} &= m\dot{\bar{V}} + \bar{\Omega} \times \bar{V} \\ \bar{M} &= \mathbf{I} \cdot \dot{\bar{\Omega}} + \bar{\Omega} \times (\mathbf{I} \cdot \bar{\Omega}) \end{aligned} \tag{2-1}$$

Assuming the quadrotor to be a rigid body with a plane of symmetry through the xz-plane, will result in the equations of motions as given in 2-2. X, Y and Z are the external forces on the rigid body, and L, M and N the external moments due to aerodynamics and actuators, all presented in their respective x, y and z directions of the body frame. See Appendix A for an overview of reference frames used.

$$\begin{aligned} -Wsin\theta + X &= m(\dot{u} + qw - rv) \\ Wcos\theta sin\phi + Y &= m(\dot{v} + ru - pw) \\ Wcos\theta sin\phi + Z &= m(\dot{w} + pv - qu) \\ L &= I_x \cdot \dot{p} + (I_z - I_y)qr - J_{xz}(\dot{r} + pq) \\ M &= I_y \cdot \dot{q} + (I_x - I_z)pr - J_{xz}(p^2 - r^2) \\ N &= I_z \cdot \dot{r} + (I_y - I_x)pq - J_{xz}(\dot{p} - rp) \end{aligned} \tag{2-2}$$

The assumptions with respect to the Parrot Bebop are as follows below. These assumptions are in general often correct, as the body is made from stiff materials to reduce vibrations, as well as limiting moving parts.

- Body is symmetric in the xz-plane. Neglecting minor fabrication mistakes, misalignments and rotor stance, the configuration is otherwise symmetric in the xz-plane.
- The drone has a constant mass. Using a battery, no fuel is required and no propellants or parts are ejected or added during flight.
- The drone has a constant moment of inertia. This implicitly assumes no moving parts. Effects from the rotating rotors are modelled separately with additional external moments.

2-2 Dominant control factors

The second level of fidelity is dominated by the Forces & Moments (F&M) applied by the control actuators, i.e. the rotors. As the term dictates, a quadrotor is usually modelled with the four rotors acting as the main interaction with its environment. This consist of the most important factor: the direct thrust and moment generated by each rotor, as well as secondary gyroscopic and reaction moments due to rotor inertia.

2-2-1 Standard rotor thrust and moment control model

The way the resulting nonconservative forces and moments are modelled vary significantly. The standard model, as described by Mahony et al. (2012), models these as the trust and rotational drag of the four rotors. Thrust provided by each rotor depends quadratically on the rotor speed. See Equation 2-3. This is a result of momentum theory, used extensively in helicopter modelling. C_T and C_Q are then a function of the air density, rotor radius, disk area and a coefficient dependent on rotor geometry and profile.

$$T_i = C_T \cdot \omega_i^2 \tag{2-3a}$$
$$Q_i = C_Q \cdot \omega_i^2 \tag{2-3b}$$

2-2-2 Secondary control moments due to rotor inertia

Although the rotors are generally very small, their rotational velocity is significantly high enough for gyroscopic moments and reaction torques to appear and influence the dynamics. These effects are not aerodynamic in nature and are henceforth considered as part of the control factors, even though their effect is often unintentional and possibly unwanted.

In Smeur, Chu, and De Croon (2016), a Incremental Nonlinear Dynamic Inversion (INDI) controller is described for the same drone, the Parrot Bebop. The gyroscopic moment and rotor spin-up torque have been determined to have a significant effect on the attitude tracking performance. Although the function of this moment is dependent on the complete inertia of a rotor and rotational rates and accelerations in all directions, it is shown that only the I_{zz} is significant due to the high rotational rate of the rotor along this axis. Hence the additional moment for a rotor can be modelled as shown in Equation 2-4.

$$M_{r_i} = \begin{bmatrix} M_{r_{i_x}} \\ M_{r_{i_y}} \\ M_{r_{i_z}} \end{bmatrix} = \begin{bmatrix} I_{r_{zz}} \Omega_y \omega_{i_z} \\ I_{r_{zz}} \Omega_x \omega_{i_z} \\ I_{r_{zz}} \dot{\omega}_{i_z} \end{bmatrix} \tag{2-4}$$

It is however noted by Smeur et al. (2016) that due to the high-frequency content of those signals, timescale separation can be used to decouple these effects from others. His high-frequency controller has a significantly increased tracking performance by incorporating this approach.

2-3 Dominant aerodynamic effects

The third level of fidelity consists of varying important aerodynamic effects as determined by leading Unmanned Aerial Vehicle (UAV) researchers. These effects are ever present and can already account for most of the aerodynamic forces experienced by drones. They are applicable to any multirotor vehicle with small single-pitch rotors and a body.

2-3-1 Blade flapping

The model is expended by G. M. Hoffmann et al. (2011) by introducing the rotor flapping and induced drag. This effect is furthermore modelled for quadrotors and experimentally identified in Huang, Hoffmann, Waslander, and Tomlin (2009) and G. M. Hoffmann et al. (2011). Here, the effects of blade flapping are modelled as a change in the inclination of the rotor plane, away from the free stream velocity. The inclination is very dependent on the stiffness characteristics of the blades.

The result of blade flapping is a longitudinal thrust, that is orthogonal to the nominal thrust vector, and can be seen as a drag force slowing the aircraft down. Mahony et al. (2012) indicates that this force is non-negligible even for low speeds and is a major factor in its natural stability of the horizontal dynamics. Mahony also states that it is a dominant aerodynamic factor in the xy-plane, which is underactuated without the reorientation of the rotors.

$$\begin{bmatrix} F_x \\ F_y \end{bmatrix}_i = T_i \left(\frac{1}{\omega_i R} \begin{bmatrix} A_{1c} & (-1)^{(i-1)} A_{1s} \\ (-1)^i A_{1s} & A_{1c} \end{bmatrix} \right), i = 1, 2, 3, 4 \tag{2-5}$$

2-3-2 Effective thrust

During climbing or descending flight, sometimes also called the heave flight condition, the rotors experience a change in the influx of wind flow. Using momentum theory, a number of models are derived to approximate the effect. The effect usually entails that thrust is increased in climbing flight and decreased in descending flight. These also described by Mahony et al. (2012) and G. M. Hoffmann et al. (2011). However, the effect is not purely dominated by a vertical inflow of air and under a varying angle-of-attack, this effect is expected to change in a non-linear fashion.

Using momentum and blade theory, the authors of those papers derived that based on the induced velocity ν_i versus the induced velocity at hover ν_h. This relationship requires solving Equation 2-6. The solution for the induced velocity varies based on the flight condition. Three important modes are identified: rapid descend, climb and the Vortex Ring State (VRS). The latter is only approximated by a parametric function and is said to be cyclically stochastic in nature, often a source of high-frequency vibrations in the vehicle, see Foster and Hartman (2017).

$$\nu_i = \frac{\nu_h^2}{\sqrt{(\nu_\infty cos\alpha)^2 + (\nu_i - \nu_\infty sin\alpha)}} \tag{2-6}$$

In Powers, Mellinger, Kushleyev, Kothmann, and Kumar (2013) the thrust provided by a single rotor is modeled as seen in Equation 2-7. This provides some insight into the effects in climbing or forward flight. A parametrized version, keeping atmospheric parameters constant, was fitted to their dataset and proved sufficiently accurate on a test rig. This equation can be linearized around a set of atmospheric conditions.

$$T_i = \frac{\rho abc\omega_i^2 R^3}{2} \left(\frac{\theta_r}{3} + \frac{V^2 cos^2\alpha\theta_r}{2\omega_i^2 R^2} + \frac{V sin\alpha + \nu_i}{2\omega_i R} \right) \tag{2-7}$$

2-3-3 Parasitic and induced drag

The standard model for drag in aircraft theory has always been related to V^2, see for example G. M. Hoffmann et al. (2011); Luukkonen (2011); Mahony et al. (2012). In quadrotor literature, this term is often modelled linearly, in order to have some account for drag. This method is considered valid due to blade flapping, which up to the speeds most applicable for quadrotors (¡5 m/s), remains mostly linear in the horizontal plane. These linear terms are used both for the induced drag hub force for each rotor, as well as the parasitic drag of the body.

However, recently Foster and Hartman (2017) has indicated that the parasitic drag in most their cases is still correlated to V^2. Their tests include the high-speed region, using a F&M test rig in wind tunnel conditions.

2-4 Additional aerodynamic effects and residuals

Subtracting the other effects mention in this chapter, the residual will probably still entail significant aerodynamic effects that are more prevalent when not in the nominal hover or climbing flight conditions. Effects that are suspected to have this effect include: body-rotor or rotor-rotor interactions will occur at higher flight speeds, changed aerodynamic parameters during compromised circumstances, imbalances during varying rotor speeds, aggressive manoeuvres (high rotational rates and accelerations) effects and possibly many others. Literature found on these effects is discussed in the following subsections.

2-4-1 Literature on the rotor wake effects

A mathematical model is presented for a quadrotor in forward-flight based one wake interference is presented by Luo, Zhu, and Yan (2015). They indicate that during high-speed flying the performance of attitude control and trajectory tracking is still unsatisfactory. Their model is based from Computational Fluid Dynamics (CFD) analysis.

2-4-2 Blade flapping effects in the lateral direction

It is noted in earlier research that in the analysis and modelling of the blade flapping lateral F&M are assumed negligible, due to the vehicle symmetry. This would thus not hold true in compromised circumstances, and must thus be taken into account. See also G. M. Hoffmann et al. (2011) and Equation 2-5.

Chapter 3

Flight path reconstruction and state estimation

Data filtering is the essential next step. Data from the sensors have to be corrected and converted into the desired state information. In the past, various sensors, filtering and fusion algorithms have been used for the quadrotors. From the literature on quadrotor models, it follows what information on the vehicle and actuator states, as well as the air flow, is important to estimate accurately. This chapter focuses on literature that solves that problem.

Although system identification techniques are available to directly estimate the system parameters from sensor data, the two-step method, as originally conceived by Mulder (1986) was introduced to improve the quality of state estimates, before applying the identification step. This is commonly known as flight path reconstruction and consists of filtering and fusing the sensor data to establish a coherent dataset from which the dynamics of a system can then be identified. This can separate the difficult nonlinear problem into easier to solve problems.

With the availability of a multisensor system, data fusion will be an essential tool. The onboard sensors available are among others: accelerometer, gyroscope and Global Position System (GPS). With testing to be done indoors, will prevent the use of GPS as external position system. However, this can be replaced by motion tracking equipment. Currently available is the Optitrack motion capture system, implemented in the TUDelft Cyberzoo. This provides a useful external observer to complement and correct for noise and bias. Exact specifications on the Bebop can be found on the Paparazzi wiki, *Bebop - PaparazziUAV* (n.d.) and other details in Appendix **??**.

This chapter provides insight into existing solutions and suitable alternative algorithms. Section 3-1 focuses on the existing use of Kalman Filter (KF)s in quadrotors and in combining sensor data. The second section focuses on alternative filtering methods.

3-1 Sensor fusion in quadrotors and robotics

In the field of robotics and state estimation in general, the KF is well established as a tool. In a survey by Chen (2012) it is stated that over 20 kinds of KFs have been implemented and documented in over 800 implementations ranging 30 years.
From the KFs, the Extended Kalman Filter (EKF) is a common tool in the field of robotics and UAV's. It allows the use of a nonlinear model and can provide a stable estimate. These models range from various sensor fusion to utilizing extensive vehicle-dynamics models to predict and correct state estimates. An example implementation is given by !!!citation!!!

With the availability of an external observer, Optitrack, new possibilities arise that replace GPS functionality. This system measures markers on the drone and tracks its position and attitude in the inertial frame. In Armanini, Karásek, de Croon, and de Visser (2017) data from onboard and off-board measurements have been time-resolved and fused using an EKF that is based on kinematic modeling. The latter fact implies no assumptions are made in the prediction of the next state of the vehicle in question. It has also been successfully used in the system identification of flapping micro aerial vehicles in Karasek, Koopmans, Armanini, Remes, and de Croon (2016) Armanini, de Visser, and de Croon (2015).
Synchronization of the time vector between the two sources is nontrivial. The synchronization is described in Karasek et al. (2016), where the synchronization is done through an active LED marker, the status of which can be read by the motion capture system. Alternatives to this strategy include correlation of the signals to an estimation of the time warping and delay.

3-2 Suitable alternatives

As a general tool, the Unscented Kalman Filter (UKF) has recently seen an increasing use in similar cases as the EKF. Conceived by Wan and Van Der Merwe (2000), the UKF uses the Unscented Transform to find the predicted distribution of points. Although computational complexity appears to be similar or slightly better than that of the EKF, its main advantage lies in avoiding the derivation of Jacobian matrices, and is better suited to deal with nonlinearities between discrete time steps.

A sensor fusion between the Inertial Measurement Unit (IMU) and GPS using the UKF is seen in Merwe and Wan (2004). The application is UAV rotercraft as a platform. Compared with the EKF it is stated that the UKF even has superior performance in dealing with the asynchronous and lagged sensor measurement. It must however be noted that higher quality IMU equipment was used.

Alternatively to the KFs that dominate the industry, complimentary filters have also seen use in quadrotors, see Mahony, Hamel, and Pflimlin (2005, 2008) uses the filter for low cost IMU measurements. Using the frequency content of such filters and smart bandwith filters, biases and noise can both be minimized. This method was primarily developed for low computing power machines, but due to its ease can be utilized as first order filter or verification.

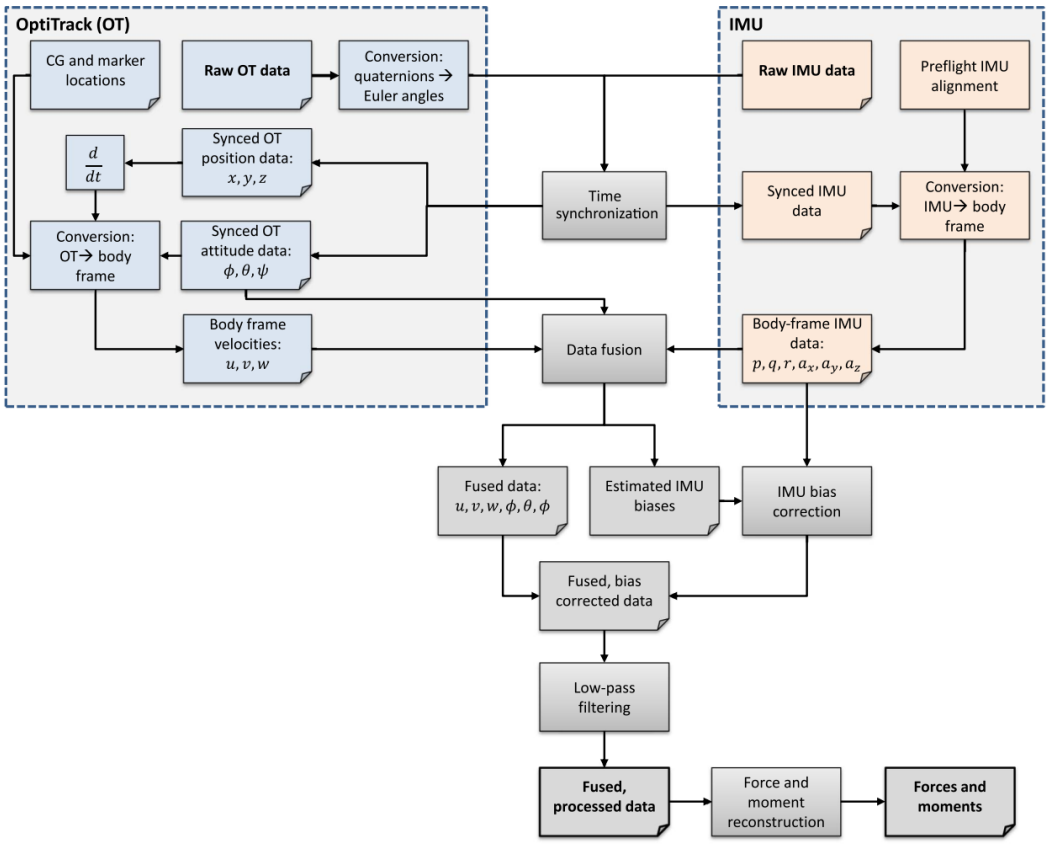

Figure 3-1: Proposed filtering scheme by Armanini et al. (2017) for fusing Optitrack motion capture data with onboard sensors

Chapter 4

Quadrotor system identification

The focus in this chapter is on the existing literature concerning system identification in the fields of quadrotors. The goal is to find both existing applications concerning problems and solutions regarding quadrotors, as well as suitable uses of system identification in other fields. Primarily this will consist of drawing parallels between the dynamics of quadrotors and aircraft or rotorcraft and the identification there-off.

As the model of the quadrotor changes, so does the appropriate method of identification. A multiple have been seen in literature regarding quadrotors or multicopters. Parametric models are the most evident, providing a white-box framework. Some research has also been seen in effectiveness modelling, motor dynamics identification and some windtunnel testing.

As established in Chapter 2, the quadrotor model in this research will differentiate in inertial properties of the body and the forces and moments applied. As such, the inertial properties will have to be able to identified separately to establish what accurate forces and moments on the body will have been as seen from flight data.

Various methods have shown the applicability to identify parameters and models in research (Hoffer, Coopmans, Jensen, and Chen (2014); X. Zhang, Li, Wang, and Lu (2014)). This chapter firstly attempts to answer the question to identify quadrotor inertial properties.

4-1 Identifying the inertia tensor for a quadrotor

It was established in Chapter 2 that the core of any model is the F&M governing the states through rigid body dynamics, along with the assumptions that can be made. Various implementations have been found in accurately determining the inertial properties, of which this section demonstrates a few. From the review in literature, three options appear viable.

It is here that it must be stated that the research subject in question, the Bebop, includes dampers that divide the vehicle into two bodies. One frame attached to the rotors and on top fuselage body containing batteries, electronics and the camera. It is however assumed

that the intrinsic shape will not change during flight and inertia properties remain the same. This assumption will have to be investigated for if its effects are non-negligible or not.

The first is the measuring of individual components, making assumptions on their mass distribution and shapes. Using the analytic equations for inertia, Mendes, Kampen, and Chu (2012) generate inertia estimates. Mendes et al. (2012) show that, with the inclusion of simplified assumptions on the inertial properties of individual components can give up to 5% accurate results. This has been tested on a similar platform and is validated by subjecting the vehicle to a F&M sensor under controlled rotations, using relatively expensive F&M sensing equipment.

In Derafa, Madani, and Benallegue (2006) a method is suggested where the vehicle is suspended by two to four wires as a pendulum. From inertial modeling an estimation is made on the expected The accuracy of this method was identified to be within 5% bounds.

The UKF has also been seen to identify quadrotor parameters. In Abas, Legowo, and Akmeliawati (2011) the UKF is seen as a method to identify a inertial quadrotor model, with body and rotor inertia. The rotor lift and drag are estimated in advance. These are then used in a nonlinear model with the inertial properties as unknown states. Given enough flight data this allows the UKF to converge to a stable estimation. This method can be used as a viable tool to check the inertial parameter values with that of other methods. However, assumptions on the aerodynamics can indirectly influence system identification results, introducing bias. Therefor a experimental methods as above are prioritized.

4-2 Identification of the rotor dynamics

Motor dynamics are important to understand the relation between the given input and the subsequent rotor speed. This can be used to further improve controllers, but also serves as a tool for improved motor state estimation.

A identification of motor dynamics is done in Pounds, Mahony, and Corke (2007). Here the motor output to input is modeled by a linear transfer function with two poles and one zero. These type of linear approximations are very common in quadrotor literature, but does not take into account saturation and other effects.

In Derafa et al. (2006) modeling of the rotors is done through linear regression. The output rpm is related to the input voltage a regressor model and solved using Least Squares (LS). The corresponding regressor matrix is shown in Equation 4-1. The resulting model parameters can be expressed in constants for rotor drag, inertia, electronic and machenical torque, and solid friction.

$$A = \begin{bmatrix} 1 & \omega & \omega^2 & \dot{\omega} \end{bmatrix} \tag{4-1}$$

These models show that often linear models are sufficient in modeling the motor dynamics. Considering the vastly smaller time-scale with other dynamics in the system, state related changes to these parameters can mostly be neglected. In the case of the rotor drag it can also be enhanced by later findings.

4-3 White-box identification of quadrotors or first-principle models

In the modeling Chapter 2 various papers have already been described that derived parameterized models of their quadrotors. The identification procedures vary between the use of LS, maximum-likelihood estimators, genetic optimization algorithms and KFs for parameter estimation.

A time domain identification procedure was carried out in Gremillion and Humbert (2010). A linear regressor based model was derived expressing states and their derivative in linear terms. The states and their derivatives were represented in state space format, with linear terms approximating forces and moments. Inputs were simulated as the mean force and the mean moments from the rotors. Although limited in its fidelity, this method proves interesting in finding poles, stability and eigenmodes of the approximated system. Windtunnel flight is still recommended as test data, as a insufficiently large test section was used.

4-4 Frequency domain identification

In Wei, Schwartz, and Cohen (2014) a linear approximation through frequency domain analysis is initiated. The system is controlled by a varying frequency sinusoidal input, or frequency sweep. Although the model is described as robust (X. Zhang et al. (2014)), the modeling method does require a lot of decoupling the various states and inputs.

4-5 Stepwise regression analysis

Stepwise regression analysis, a technique presented in Klein and Morelli (2006), is a method of system identification that establishes a regressors based model based on a pool of dependent variables. A choice must be made for the model structure. A suitable model structure must be linear-in-the-parameters, such as a polynomial model. A selection can then be made out of a pool of regressors, and allow combinations, such as $V^2\alpha$.

This type of analysis iterates over the pool of regressors. Using least squares the parameters are calculated. The F-test can be used to identify if a regressor contributes significantly to the model quality, regressors are added or eliminated until a stop criteria is reached. A suitable criteria will have to be selected and tuned.

The benefit of using this method is that predefined standard regressors can be added, such as likely candidates for blade flapping and incoming flow. Regressors can be nonlinear as long as the parameters remain linear, such that least squares methods can be used to efficiently estimate parameters and their quality, as defined by the parameter variance.

4-5-1 Stepwise Regression Analysis algorithm

The main goal of structure selection process is finding specific regressors from a regressors candidate pool, to form up the final model. The candidate pool are formed by possible combinations of independent variables. This combination can be in any formation, for example,

log function, exponent function, etc. In this paper, the polynomial function is used to form regressors pool. For instance, if the preliminary model structure is organized as Equation 4-2 from prior knowledge

$$y = P_1^2(x_1, x_2) + P_2^2(x_1, x_2)x_3 \tag{4-2}$$

where $P^2(x_1, x_2)$ stands for the second order polynomial function. Then the candidate pool contains all kinds of combinations of independent variables. In this example, candidates should be x_1, x_2, x_3, x_1^2, x_2^2, x_1x_2 and x_1x_3, x_2x_3, x_3x_3, $x_1^2x_3$, $x_2^2x_3$, $x_1x_2x_3$. Generally, for a dth order polynomial function with n independent variables $P^d(x_1, x_2, ..., x_n)$, the total number of terms in the candidate pool is shown in Equation 4-3.

$$\hat{d} = \frac{(d+n)!}{n!d!} \tag{4-3}$$

After defining the candidate pool, the forward-backward stepwise selection process is described in the following steps to select qualified regressors to form up the model.

- INIT:
  The model starts from the simplest form with only constant (bias) term

$$z = A\theta_0 + \epsilon, \quad A = \begin{bmatrix} 1 \\ : \\ 1 \end{bmatrix} \tag{4-4}$$

- LOOP:

  1. Estimate parameters in the model by Equation 4-5. And compute the model residual
  $$\epsilon = z - A\hat{\theta} \tag{4-5}$$
  2. For each candidate regressor in the pool, remove part of it until the rest is orthogonal to the terms already in the model. This process is achieved by using least square method. Specifically, for regressor ξ_i in the pool, the rest part after this removal equals
  $$\lambda_i = \xi_i - A(A^TA)^{-1}A^Tz \tag{4-6}$$
  3. Select the index j with which λ_j has the highest correlation with current model residual ϵ. Add candidate ξ_j as a new column of regressor matrix A.
  4. Evaluate existing regressors in the model by F test. Assume there are already p regressors in the current model. The partial F-ratio for the kth regressor is
  $$F_0 = \frac{SS_R(\hat{\theta}_p) - SS_R(\hat{\theta}_{p-k})}{s^2} \tag{4-7}$$
  where s^2 is fit error variance computed by
  $$s^2 = \frac{\epsilon^T\epsilon}{N-p-1} \tag{4-8}$$

$SS_R(\hat{\theta}_p)$ stands for the regression sum of squares for current model, and $SS_R(\hat{\theta}_{p-k})$ stands for that of the model after eliminating the regressor ξ_k. The formula for regression sum of squares is

$$SS_R = \hat{\theta}^T A^T z - N\bar{z} \tag{4-9}$$

where $\bar{z}$ is the mean of measurement z. If ξ_i is the regressor with the least F_0 and

$$F_0 < F_{out} = 4 \tag{4-10}$$

then this regressor is eliminated from the current model. If ξ_k is exactly the regressor selected in the last step, stop the algorithm.

- STOP CRITERION:
  Predict square error (PSE) is selected as the stop criterion in this research.

$$PSE = \frac{1}{N}\epsilon^T\epsilon + \sigma^2_{max}\frac{p}{N} \tag{4-11}$$

The first term is the mean square fit error for the modeling data, and the second term is the penalty term for model redundancy. The penalty coefficient is chosen as

$$\sigma^2_{max} = \frac{1}{N}\sum_{i=1}^{N}[z(i) - \bar{z}]^2 \tag{4-12}$$

More regressors in the model, i.e larger p, the penalty term will contribute more for PSE. Thus as there are more regressors added into the model, the PSE will decrease at the beginning and finally increase. Thus if

$$PSE \geq PSE_{last} \tag{4-13}$$

the algorithm stops to avoid over-fitting.

4-6 Multivariate spline models

A newer method of system identification in the field of aviation is that of using multivariate splines, see de Visser, Chu, and Mulder (2009). This type of modeling has also been applied to quadrotor thrust variance by Visser, De Visser, and Van Kampen (2015). The benefit of this type of modeling is in the applicability of approximating high dimensional and nonlinear data, if the amount of data is high enough. Model information can be introduced through constraints. This process can especially benefit from the known model literature on quadrotors, allowing for a very accurate baseline model.

This type of system identification is especially useful when paired with the stepwise regressor selection, taking advantage of the correlation data to select for which dimensions a dataset has to be analyzed, in order to efficiently map all forces and moments with the selected states. The downside of this approach is the difficulty in gaining insight in four or higher dimensional model structures, requiring subsets to be evaluated by the model designer. Then there is also the difficulty in selecting a sufficient triangulation, for which only a select amount of very general methods are available.

Chapter 5

Quadrotor control

With the envisioned approach on flight testing damaged systems, it is essential to implement controllers that are fault tolerant. New approaches can even still fly quite efficiently. What options are available and how they work is discussed in this Chapter.

5-1 Fault tolerant controllers with compromised actuators

In work done by Mueller and D'Andrea (2014) it is shown for the first time that quadrotors with sufficient control power can be stabilized and brought down gently after an accident with 1 propeller or 2 opposing propellers. A special case is also possible for a case where 3 propellers are compromised, but is noted to be unrealistic for standard designs. A quadrotor used the 4 propellers to control 4 Degree of Freedom (DOF), and indirectly can move laterally. If one or more rotors are compromised, the drone loses its ability to control the yawing motion, due to the lack of equilibrium between the remaining rotors. Due to various assumed aerodynamic effects a stabilizing influence is added to the yawing motion of a quadrotor. This allows a controller to enter a state of continuous but stable spinning motion, while maintaining altitude and pitch and roll control. A Linear Quadratic Regression (LQR) conroller was designed by Mueller and D'Andrea (2014) that demonstrates this effect successfully. In this controller, the stabilizing influence is assumed to be a linear drag term w.r.t. yawing rotational velocity r, combined with a standard model of second degree fidelity (see Chapter 2) of the quadrotors actuators.

5-2 Incremental Nonlinear Dynamic Inversion control

During the '90s, the INDI controller scheme has been suggested as an improvement on the Nonlinear Dynamic Inversion (NDI) scheme, see Smith (1998), Bacon and Ostroff (2000). Instead of using a complete global model, as used in NDI, INDI uses the sensors to provide information on the current state of the vehicle. The controller then uses a model describing the

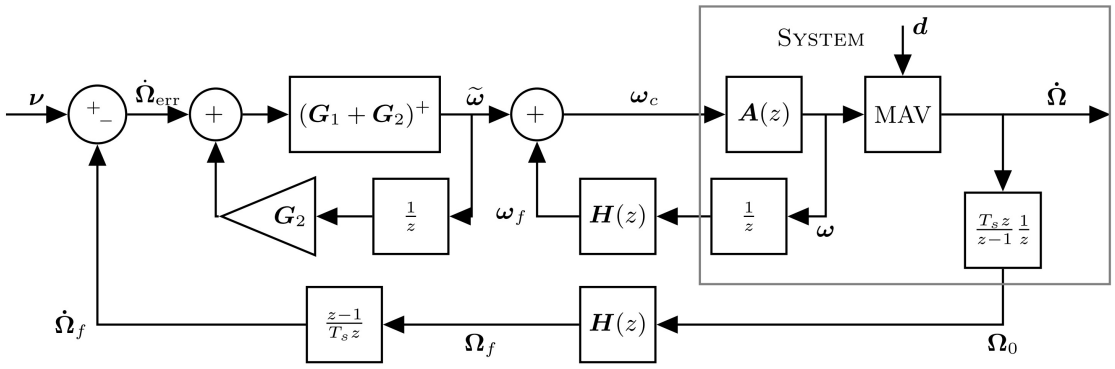

Figure 5-1: INDI controls scheme as by Smeur et al. (2016). A(z) denotes the actuator dynamics, H(z) a second order filter, G_1 and G_2 the control effectiveness matrices. The formulation is expressed in the z-domain to indicate the discrete time approximation with T_s being the sample time.

relation between those states and the actuators, often referred to as the control effectiveness model.

Recently this scheme has been adapted by Smeur et al. (2016) for the Parrot Bebop. This new adaptve INDI controller uses a control effectiveness model and uses estimates of the angular accelerations from MEMS sensors to replace the rest of the model. Besides dealing with the filtering and control delays, the controller's control effectiveness matrix is identified in real time, allowing the controller to adapt to new situations. In his paper it is shown that in-flight modifications to the vehicles mass distribution and windtunnel gusts are compensated for in real time, allowing for more precise control in varying conditions experienced across the flight envelope. Outer-loop control is done through linear PD control of the angles and angular velocities.
The vehicle model takes into account rigid body dynamics, rotor inertia and momentum and the standard model for rotor thrust and drag. The control effectiveness matrix is then derived from this model, and subsequent parameters do not necessarily relate the the real world parameters such as inertia. The author notes yaw control is especially improved due to the inclusion of rotor momentum. An overview of the inner loop of the INDI controller is shown in Figure 5-1.

In recent unpublished work by Hoppener (2016), the INDI controller as proposed by Smeur et al. (2016) is changed to incorporate a Weighted Least Squares (WLS) control allocation scheme. The scheme and subsequent implemented controller (also on the Parrot Bebop) allows for the controller to give weights to certain control objectives. Subsequently, stability and altitude control can be more important than maintaining heading and solves the control tracking fault experienced in roll, pitch and altitude experiencing during a high magnitude yaw maneuver. The scheme is also augmented with a thrust effectiveness, related to the A_z, the acceleration experiencing in the body z-direction, allowing for the INDI to control and adapt for altitude control.
More importantly, through experiment it is shown that this controller can maintain stability during a compromised actuator event. A rotor has its radius reduced, thus introducing the yaw control imbalance. The vehicle enters the stable yaw rotation state as described by Mueller and D'Andrea (2014). During this time the INDI controller learns the new effectiveness of

the actuators and compensates through the WLS control allocator to remain stable, as long as $W_r \gg W_p, W_q$ and W_{thrust}.
It is noted that the controller is required to adapt quickly to the new actuator situation. Pre-learning possibilities are noted as an option in further use, as well as recommending improvements on the learning abilities of the controller, such that knowledge of physical bounds can be incorporated. Although the controller takes into account actuator saturation, it is noted that those limits can change for a compromised actuator, allowing for higher actuator speeds to compensate.

Chapter 6

Methodology

To achieve the research objective, namely the identification of a damaged drone, choices must be made in the methods used to achieve it. This includes the methods to obtain accurate data, model structure and system identification tools and statistical tools to validate the results obtained. Which ones are selected is discussed in this Chapter.

6-1 Flight path reconstruction

The first step in data analysis is the reconstruction of a true state estimate. To this end the Extended Kalman Filter approach is selected to combine information from multiple sensors and sensor accuracy statistics. The basis of this approach is taken from Armanini et al. (2017), who graciously also provided the accompanying code.

Time synchronization is done by doing a correlation analysis between states measured from onboard and offboard sensors. This can be done by correlation multiple states, such as measured rotational velocity, accelerations or logged position. Data is sent from the offboard system to the drone to provide position control. This information can be logged and used as well. This differs to the synchronization in Karasek et al. (2016), where the synchronization is done through an active LED marker.

Delay and clock drift can be identified using a dynamic time warping analysis to minimize the clock errors/delays involved. In the event of insufficient performance, the onboard gps clock can be used as a third reference.

The EKF approach utilizes the kinematic relation between the acceleration and rotational rate measured from the onboard IMU and the observed attitude and velocity from the Optitrack system. Here it is assumed that the velocity can be safely derived from the position due to its accuracy. The EKF has 12 states, including 6 bias terms for the IMU that are identified, as they slowly change over time. A 4th order butterworth filter can be applied to reduce vibrations evident from unwanted dynamics.

6-2 Force and moment estimation

To estimate the forces and moments during flight it is of vital importance to have an accurate mass model available and to deduce the moments and products of inertia. The Bebop is assumed as a rigid body, symmetrical in the xy plane (body reference). Its mass and inertial properties are constant over time. As such the required inertias are: $I_{xx}, I_{yy}, I_{zz}, J_{xz}$.

It is here that it must be stated that the research subject in question, the Bebop, includes dampers that divide the vehicle into two bodies. One frame attached to the rotors and on top fuselage body containing batteries, electronics and the camera. It is however assumed that the intrinsic shape will not change during flight and inertia properties remain the same. This assumption will have to be investigated for if its effects are non-negligible or not.

The external forces and moments can then be deduced by inverting Equations 6-1 and 6-2, since all other states are known. Here $\vec{G}$ is the gravitational force.

$$m \begin{bmatrix} \dot{u} \\ \dot{v} \\ \dot{w} \end{bmatrix} = m \begin{bmatrix} p \\ q \\ r \end{bmatrix} \times \begin{bmatrix} u \\ v \\ w \end{bmatrix} + \vec{G} + \vec{F} \tag{6-1}$$

$$\mathbf{I_v} \begin{bmatrix} \dot{p} \\ \dot{q} \\ \dot{r} \end{bmatrix} = \begin{bmatrix} p \\ q \\ r \end{bmatrix} \times \mathbf{I_v} \begin{bmatrix} p \\ q \\ r \end{bmatrix} + \vec{M} \tag{6-2}$$

where u, v, w indicate the velocity components expressed in body coordinate system, and p, q, r stand for angular speed with respect to the three axis. m and $\mathbf{I_v}$ represent mass and inertia matrix respectively. $\vec{G}$ is gravity vector. $\vec{F}$ is the resultant force except gravity and $\vec{M}$ is the resultant moment on quadrotor.

6-3 Model structure

The chosen system as to be identified is a rigid body undergoing forces and moments. The relationship between the forces and moments and the system states is defined as the aerodynamic model. Using the two-step method, this allows for a nonlinear state estimate with the EKF and linear in the parameters model for the force and moment estimation.

Multiple model structures will have to be considered and fitted to the data. The first model is evidently the basic model found in literature, modeling the forces and moment generated by each actuator as $f(\omega_k^2)$. Further models can incorporate more terms, such as the inertial forces generated by the rotors (gyroscopic effect) Smeur et al. (2016), effects of inflow of air into the rotor disks Huang et al. (2009),G. M. Hoffmann, Gorinevsky, Mah, Tomlin, and Mitchell (2007).

6-4 Stepwise regression analysis

Stepwise regression analysis, a technique presented in Klein and Morelli (2006), is a method of system identification that establishes a regressors based model based on a pool of dependent

variables. A choice must be made for the model structure. In the case of this project, a polynomial structure is used. Up to a to be selected degree, dependent variables can be used or combined to form polynomial regressors, for example $V^2\alpha$.

The analysis iterates over the pool of regressors. Using least squares the parameters are calculated. Using the F-test to identify if a regressor contributes significantly to the model quality, regressors are eliminated until a stop criteria is reached. To be selected criteria will have to be defined for what a good candidate will be.

The benefit of using this method is that standard regressors can be added, such as predefined, possibly nonlinear effect for bladeflapping or incoming flow as known from literature. Regressors can be nonlinear as long as the parameters remain linear, such that least squares methods can be used to efficiently estimate parameters and their quality, as defined by the parameter variance.

Chapter 7

Experiment design and execution

The free-flight wind tunnel experiment is at the centre of this research, with most of the months leading up to it being focussed on its preparation. Up to that point, the focus was on the selection of sensor fusion, configurations and suitable controllers. Test flights have been flown at the TUDelft Cyber Zoo to ensure all requirements were met. The resulting experiment is described in this chapter.

The free-flight wind tunnel experiment was flown at the Open Jet Facility (OJF) of the TUDelft in March 2017. Two Bebop drones flew in varying wind velocities and directions, in five different configurations. During these tests, data was gathered from inertial onboard sensors and ceiling mounted OptiTrack cameras. The gathered data is filtered using the EKF, and resulting accelerations give the forces and moments.

This chapter provides an overview of the experiment setup. This includes the data gathering setup, implemented controller, wind tunnel characteristics and flight plan. Also, some data-specific filtering is described, and inertial parameter estimation. This chapter discusses in depth the experimental conditions, controller design, manoeuvre design and sensor data gathering and filtering techniques used. First the experimental platform, the Bebop is discussed. Secondly the chosen experimental conditions. It is followed by a description of the OJF with insight on velocity flow field and external sensor placement. Fourthly the OptiTrack system is discussed, followed by a description of the sensor filtering techniques used to estimate states from both external and onboard sensors. Lastly, the manoeuvres are evaluated by onboard controller, navigational strategy and controller tuning, with insight to towards the set of states reached.

7-1 Experimental platform, the Parrot

The selected quadrotor as the experimental platform is the Parrot Bebop, a quadrotor equipped with an integrated camera for photos and videos. The native software is replaced by Paparazzi, an open-source autopilot platform. For their wiki, see *Paparazzi Wiki* (n.d.)

and their repository; *Paparazzi Repository* (n.d.). The autopilot runs on a 512Hz loop, estimating the state using its various sensors, sending control commands and logging desired information.

The relevant sensors available to the Bebop include a 3-axis accelerometer and a 3-axis gyroscope (MPU 6050), commonly referred to as the IMU. Its rotors are closed-loop controlled brushless rotors. They use counter electromotive force (back-EMF) to control the rotor rate and provide data. During the experiment, the accelerometer, gyroscope and rotor rate values are logged at 512Hz.

The frame of the Parrot Bebop consists of two parts. The upper body contains the sensors, battery and other computing equipment. Through four spring-dampers these are connected with the rotor frame, which connects to all the rotors. The dampers are necessary to damp high-frequency vibrations from the rotors but induce unwanted dynamics in the sensors. This is a problem to be addressed in the filtering and should be carefully considered in any model that catches high-frequency dynamics.

7-2 Open Jet Facility wind tunnel and flow characterization

For subjecting the quadrotor to constant wind velocities, the OJF at the TUDelft was used. This wind tunnel is the largest available to the TUDelft and circulates air through a tunnel using a turbofan. The wind tunnel has an outlet aperture of effectively 3m in diameter, where the outlet cross section is a 285x285cm octagonal. After the entering large test section, the flow is sucked through a cooler and back into circulation, hence controlling the atmospheric conditions. The schematics can be seen in Figure 7-1b.

The outlet of the tunnel into the test chamber was covered with a fence to prevent the drone from entering the tunnel itself. No notable disturbances in the flow were detected. The quality of the flow was inspected both visually by woollen tufts and by measuring flow velocity with pitot tubes. The end of the test chamber and the cooler were protected by a net. The resulting usable test section for measurements was 2.5 meters wide and 5 meters long, starting 1 meter behind the outlet. The test section can be seen in Figure 7-1a.

The quality of the wind tunnel flow has been subject to previous research by Lignarolo et al. (2014). Here, an angled aperture of 9.5° for the shear layer was found. This resulted in a free-stream area reduction of $16.7 cm/m$ behind the aperture. At 6m the usable area is 2x2 m. It was also found that at 1 m behind the aperture, the mean flow velocity is diminished by 1% and 3% at 6 m. The wind tunnel velocity is corrected by assuming a linear diminishing flow quality between 1 and 6 meters. Any results obtained outside of the determined free-stream velocity field are discarded and not used for data analysis.

7-3 External position and attitude estimation

External position and attitude were measured by 10 OptiTrack Prime 17W cameras. They observe the 2D location of reflective markers placed on the body and rotors of the Bebop. The cameras were set to record, at 360fps, the locations of these markers. Using Motive 1.10.2 the information of each camera is combined to reconstruct the 3D marker data. A set of 3D

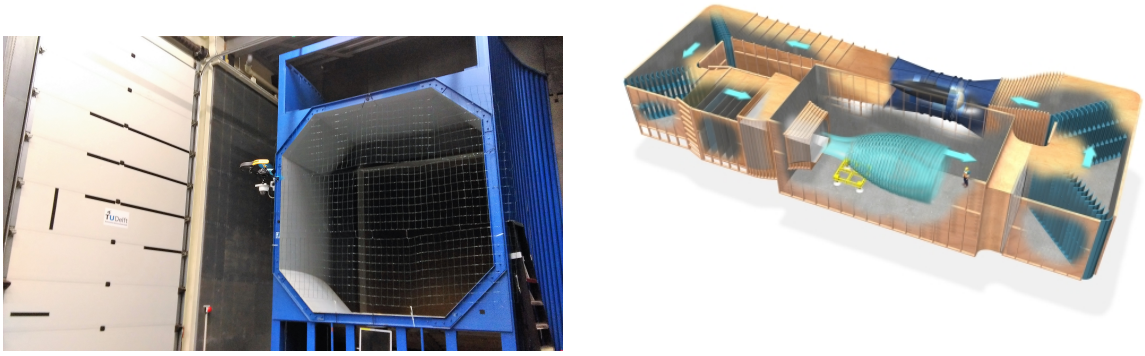

(a) Photo taken during the experiment. **(b)** Schematic of the Open Jet Facility.

Figure 7-1: The photo on the left shows test section, outlet and the Bebop flying while gathering data. Cameras are measuring the 3D orientation from the ceiling. The OJF wind tunnel schematic is shown on the right. The cyan airflow gives an idea of the test section flow expansion. The dark blue section contains the turbofan.

markers can be selected to form a simulated rigid body. This rigid body is fitted on the 3D marker data of each frame. The resulting fit gives the position and attitude of the Bebop body.

The cameras were placed at the ceiling of the test chamber, approximately 7m above the floor and 3.5m above the ideal measuring position of the drone. They were placed in a 4-2-4 pattern, looking down and inward. Combined with the individual cameras field of view of 70° this gives sufficient coverage for each marker to be viewed by multiple cameras at any given moment in the test section. Cameras were calibrated twice a day, using a wand with accurately known placed markers on it. The ground plane is set after this process, levelled with respect to the gravity vector (Optitrack y-axes) and aligned with the flow direction (OptiTrack z-axis).

Gaps in the marker data and mislabeling errors can occur frequently. Small gaps (less than 0.1s) were filled with a linear interpolation. If not enough markers were seen or if outliers were detected, the rigid body is marked as untracked and the frame is discarded. This process is automated in the Motive batch-processor. A detailed overview of the reconstruction settings is available in Appendix **??**.

7-4 Controller design and chosen commands during the experiment

The control and stabilization of the Bebop was done by utilizing the INDI controller developed by Smeur et al. (2016), adapted with a WLS control allocator by Hoppener (2016). The control objective weights were: $W_\psi, W_\theta, W_\phi, W_{thrust} = [1000, 1000, 1, 700]$. The combination of these two methods allows for responsive but disturbance-rejecting control while giving control priority to remain upright. Providing sufficient thrust is the second priority and making yaw manoeuvres is the last priority.

The quadrotor during the experiment was subjected to various magnitudes of wind velocity,

ranging between 0 and $15m/s$. The quadrotor was set to make manoeuvres along the wind flow, manoeuvres horizontally perpendicular to the flow, altitude manoeuvres and rotational manoeuvres. Longitudinal, latitudinal and vertical manoeuvres were repeated for heading angles between -180 and 180 degrees in steps of 45 degrees.

Longitudinal and latitudinal manoeuvres were achieved by setting the desired position reference. By changing controller gains and position references to different values, varying magnitudes were achieved. Vertical manoeuvres were achieved by varying the desired climb velocity between -2 and 2 m/s, limited by the test section size. Rotational manoeuvres were achieved by changing the heading reference by steps of 45/90/135/180 degrees, varying between them. The rotational manoeuvres were achieved by changing the target heading in steps between 45 to 180 degrees.

These manoeuvres were supplemented with manual or human-in-the-loop position controlled flights. These flights were focused on first repeating the flights that were made autonomously, as well as introducing larger than normal excitations to the system and perform coupled manoeuvres that were otherwise deemed too difficult to generate autonomously.

7-5 Bebop inertia estimate

In order to obtain forces and moments to be evaluated during flight, the translational and rotational accelerations need to be known, combined with an accurate mass and inertia model. This required measuring or estimating the inertia beforehand and to fuse the data from both onboard and external sensor equipment.

Using the mass and simple inertia estimates of individual components, an estimate of the inertia was established. The results are shown in Table 7-1. The process is described by Mendes et al. (2012). In Mendes et al. (2012) the inertia is determined for a similar quadrotor and validated to be within a 5% accuracy. It is expected that this error will only influence the value of resulting regressors coefficients and will not significantly influence the selection of these regressors.

Table 7-1: Mass model of the baseline Parrot Bebop. Other configurations not shown here.

Mass$[kg]$	I_xx$[kg \cdot m^2]$	I_yy $[kg \cdot m^2]$	I_zz $[kg \cdot m^2]$	I_xz$[kg \cdot m^2]$
0.38905	0.00097227	0.0008601	0.0017473	1.4178e-05

7-6 Sensor fusion and filtering

The sensor fusion and filtering is performed by the EKF as described by Armanini et al. (2017). Results and tuning of the final sensor fusion algorithm will be shown in the final thesis, so only a brief overview is given here. For a detailed breakdown of the sensor filtering approach, the reader is referred to the original work of Armanini et al. (2017) and Section 3-1.

The onboard data log and the OptiTrack frames are logged at different frequencies and require a time synchronization to be useful. Armanini et al. (2017) solved this by using a LED

marker for time synchronization between onboard and external sensors. Due to such a method being unavailable here, time synchronization is achieved by correlation. Data sent to the Bebop during flight, such as OptiTrack position data, was logged together with the inertial data. Taking into account the time delay (ping) between measuring and receiving the data onboard, this additional log can be used to infer the time delay between sensors. Additionally, correlation of states can also provide correction. Especially over long measuring times, this can be necessary to prevent clock errors from developing a bias.

The EKF fuses the onboard inertial data, rotational rate and acceleration, with the externally measured attitude and velocity data (derived from position). Onboard data is re-sampled to the OptiTrack framerate. The EKF predicts the next observation by using kinematic equations and the inertial sensor data. Next, the prediction is corrected with the external attitude and velocity measurement. Due to heavy vibrations in the onboard data, the parameters of the EKF are tuned to rely more heavily on the OptiTrack observation.

The data from the OptiTrack system contain bias terms with respect to the actual orientation and centre of gravity. Using the measured positions of each of the placed markers, the bias can be calculated. For each flight, these terms are calibrated such that the external position and attitude data correspond with the established body frame.

The corrected onboard data is fed through a 4th order Butterworth (low-pass) filter to cancel out vibrations resulting from the rotors imbalance. These vibrations are influenced by the dual body spring-damper dynamics of the Bebop. These dampers were originally placed to damp high-frequency vibrations to improve camera quality, however, introduce unwanted dynamic noise into the data.

Chapter 8

Conclusions

This thesis has documented the selected path towards fulfilling its research goal: fill the gap of knowledge on quadrotor models in compromised circumstances and high-speed conditions. This goal follows from the need for safer control algorithms for both quadrotors and aircraft in general. Safe-flight-envelope estimators are envisioned with a database approach to handle compromised circumstances for such vehicles. Those require accurate global models valid for multiple configurations. The goal encompasses a great effort and scope. Limiting that scope, the research question becomes: *How can the Parrot Bebop quadrotor dynamics be modelled for high speed and single actuator loss conditions and identified from a free-flight wind tunnel experiment using modern system identification techniques?*

In the current state-of-the-art, it is found that existing models for the quadrotor are based mostly on the basic quadrotor model. This model is often extended as the situation requires it. High fidelity models in the literature included effects such as blade flapping, thrust variation due to induced velocity, rotor inertia with gyroscopic effects, rotor hub forces and regression terms to deal with the damping effects on translation and rotation.

The goal is to estimate new models with a higher fidelity. For this to be done, system identification methods are envisioned to select a model structure and estimate model parameters directly from flight data. This stands in contrast to the use of CFD methods or first principle models. Flight data is gathered from a wind tunnel experiment, utilizing onboard inertial sensors and external reflective marker tracking cameras to establish an accurate state dataset. The information is combined used an Extended Kalman Filter, utilizing a kinematic model to incorporate sensor accuracy statistics and having the added benefit of no assumptions being made on the model during state estimation.

Flight control is handled with the INDI controller incorporating WLS control allocation to allow for the Bebop to remain stable during single actuator loss flight. Wind tunnel experiment results were successful in remaining stable up to 7 m/s under compromised circumstances and 15 m/s in the baseline configuration.

The flight data is converted to a force-moment dataset using predetermined inertial properties determined by measuring individual component weights and derive inertia through a simplified

model. The system identification step is to relate the forces and moments to the actuator and vehicle states. For this step, a regressor model structure is selected. The Stepwise Regressor Selector was chosen as an appropriate system identification tool to determine the suitable model structures.

The final result will consist of the following. First, a wind tunnel filtered dataset. Secondly, identified model structures and respective parameters for two configurations. Third and fourth will be comparisons of the two configurations among themselves and a comparison relative to models determined from literature.

The expected results are believed to improve the knowledge of the scientific community to further estimate quadrotor behaviour under varying circumstances and help to create safer and better controllers under selected configurations.

Appendix A

Reference frames used

In this appendix the reference frames as used in this project are described.

The first is the inertial frame. The origin is usually dictated as a specific point in the respective room, such as the Cyberzoo or the OJF. Depending on the situation, the x-direction is often aligned with the z-direction of the Optitrack system in the Cyberzoo or the direction of flow in the windtunnel. Otherwise the reference frame is considered a North-East-Down (NED) frame.

The second is the body frame. As is common in aerospace literature, the body frame is defined as Forward-Right-Down (FRD) frame. The origin lies in the (assumed) Center of Gravity (C.G.).

References

Abas, N., Legowo, A., & Akmeliawati, R. (2011, may). Parameter identification of an autonomous quadrotor. In *2011 4th int. conf. mechatronics integr. eng. ind. soc. dev. icom'11 - conf. proc.* (pp. 1–8). IEEE. Retrieved from http://ieeexplore.ieee.org/document/5937198/ doi: 10.1109/ICOM.2011.5937198

Armanini, S. F., de Visser, C. C., & de Croon, G. (2015, jan). Black-box LTI modelling of flapping-wing micro aerial vehicle dynamics. In *Aiaa atmos. flight mech. conf.* Reston, Virginia: American Institute of Aeronautics and Astronautics. Retrieved from http://arc.aiaa.org/doi/abs/10.2514/6.2015-0234http://arc.aiaa.org/doi/10.2514/6.2015-0234 doi: 10.2514/6.2015-0234

Armanini, S. F., Karásek, M., de Croon, G. C. H. E., & de Visser, C. C. (2017, apr). Onboard/Offboard Sensor Fusion for High-Fidelity Flapping-Wing Robot Flight Data. *J. Guid. Control. Dyn.*, 1–12. Retrieved from https://arc.aiaa.org/doi/10.2514/1.G002527 doi: 10.2514/1.G002527

Bacon, B., & Ostroff, A. (2000). Reconfigurable flight control using nonlinear dynamic inversion with a special accelerometer implementation. In *Aiaa guid. navig. control conf. exhib.*

Bebop - PaparazziUAV. (n.d.). Retrieved 2018-06-14, from https://wiki.paparazziuav.org/wiki/Bebop

Chen, S. Y. (2012, nov). Kalman Filter for Robot Vision: A Survey. *IEEE Trans. Ind. Electron.*, *59*(11), 4409–4420. Retrieved from http://ieeexplore.ieee.org/document/5985520/ doi: 10.1109/TIE.2011.2162714

Derafa, L., Madani, T., & Benallegue, A. (2006). Dynamic Modelling and Experimental Identification of Four Rotors Helicopter Parameters. In *2006 ieee int. conf. ind. technol.* (pp. 1834–1839). IEEE. Retrieved from http://ieeexplore.ieee.org/document/4237837/ doi: 10.1109/ICIT.2006.372515

de Visser, C., Chu, Q., & Mulder, J. (2009, dec). A new approach to linear regression with multivariate splines. *Automatica*, *45*(12), 2903–2909. Retrieved from http://linkinghub.elsevier.com/retrieve/pii/S0005109809004270 doi: 10.1016/j.automatica.2009.09.017

Foster, J., & Hartman, D. (2017). High-fidelity multirotor unmanned aircraft system simu-

lation development for trajectory prediction under off-nominal flight dynamics. In *17th aiaa aviat. technol. integr. oper. conf. 2017*.

Gremillion, G., & Humbert, J. (2010). System identification of a quadrotor micro air vehicle. In *Aiaa atmos. flight mech. conf. 2010*.

Hoffer, N. V., Coopmans, C., Jensen, A. M., & Chen, Y. (2014, apr). A Survey and Categorization of Small Low-Cost Unmanned Aerial Vehicle System Identification. *J. Intell. Robot. Syst.*, *74*(1-2), 129–145. Retrieved from http://link.springer.com/10.1007/s10846-013-9931-6http://search.proquest.com/openview/6a02a1f7da2edbc05b750e15f76d484b/1?pq-origsite=gscholar{&}cbl=326251 doi: 10.1007/s10846-013-9931-6

Hoffmann, G., Rajnarayan, D., Waslander, S., Dostal, D., Jang, J., & Tomlin, C. (2004). The Stanford testbed of autonomous rotorcraft for multi agent control (STARMAC). In *Aiaa/ieee digit. avion. syst. conf. - proc.* (Vol. 2, pp. 12.E.4–121–10). IEEE. Retrieved from http://ieeexplore.ieee.org/document/1390847/ doi: 10.1109/DASC.2004.1390847

Hoffmann, G. M., Gorinevsky, D., Mah, R. W., Tomlin, C. J., & Mitchell, J. D. (2007). Fault Tolerant Relative Navigation using Inertial and Relative Sensors . *Collect. Tech. Pap. - AIAA Guid. Navig. Control Conf. 2007*, *5*(August), 1–18.

Hoffmann, G. M., Huang, H., Waslander, S., & Tomlin, C. J. (2011, sep). Precision flight control for a multi-vehicle quadrotor helicopter testbed. *Control Eng. Pract.*, *19*(9), 1023–1036. Retrieved from https://www.scopus.com/inward/record.uri?eid=2-s2.0-79960891417{&}partnerID=40{&}md5=1ece5efa1742135b0b47f287f69099a9http://linkinghub.elsevier.com/retrieve/pii/S0967066111000712 doi: 10.1016/j.conengprac.2011.04.005

Hoppener, D. (2016). Actuator Saturation Handling using Weighted Optimal Control Allocation Applied to an INDI Controlled Quadcopter.

Huang, H., Hoffmann, G. M., Waslander, S. L., & Tomlin, C. J. (2009). Aerodynamics and control of autonomous quadrotor helicopters in aggressive maneuvering. In *2009 ieee int. conf. robot. autom.* (pp. 3277–3282). IEEE. Retrieved from http://ieeexplore.ieee.org/document/5152561/ doi: 10.1109/ROBOT.2009.5152561

Karasek, M., Koopmans, A. J., Armanini, S. F., Remes, B. D., & de Croon, G. C. (2016, oct). Free flight force estimation of a 23.5 g flapping wing MAV using an on-board IMU. In *2016 ieee/rsj int. conf. intell. robot. syst.* (Vol. 2016-Novem, pp. 4963–4969). IEEE. Retrieved from http://ieeexplore.ieee.org/document/7759729/ doi: 10.1109/IROS.2016.7759729

Klein, V., & Morelli, E. A. (2006). *Aircraft System Identification: Theory and Practice*. American Institute of Aeronautics and Astronautics Reston, Va, USA. doi: ISBN1-56347-832-3

Lignarolo, L., Ragni, D., Krishnaswami, C., Chen, Q., Simão Ferreira, C., & van Bussel, G. (2014, oct). Experimental analysis of the wake of a horizontal-axis wind-turbine model. *Renew. Energy*, *70*, 31–46. Retrieved from http://flow-offshore.nl/images/flow-openbaar/p201101{_}012{_}tud{_}bijlage.vi.progress.report.h1.2014{_}v01.pdfhttp://linkinghub.elsevier.com/retrieve/pii/S0960148114000494 doi: 10.1016/j.renene.2014.01.020

Luo, J., Zhu, L., & Yan, G. (2015). Novel Quadrotor Forward-Flight Model Based on Wake Interference. *AIAA J.*, *53*(12), 3522–3533. Retrieved from https://arc.aiaa.org/doi/pdf/10.2514/1.J053011http://arc.aiaa.org/doi/10.2514/1.J053011 doi:

10.2514/1.J053011

Luukkonen, T. (2011). Modelling and Control of Quadcopter. *Indep. Res. Proj. Appl. Math.*.

Mahony, R., Hamel, T., & Pflimlin, J.-M. (2005). Complementary filter design on the special orthogonal group SO(3). In *Proc. 44th ieee conf. decis. control* (Vol. 2005, pp. 1477–1484). IEEE. Retrieved from http://ieeexplore.ieee.org/document/1582367/ doi: 10.1109/CDC.2005.1582367

Mahony, R., Hamel, T., & Pflimlin, J.-M. (2008, jun). Nonlinear Complementary Filters on the Special Orthogonal Group. *IEEE Trans. Automat. Contr.*, *53*(5), 1203–1218. Retrieved from http://ieeexplore.ieee.org/document/4608934/ doi: 10.1109/TAC.2008.923738

Mahony, R., Kumar, V., & Corke, P. (2012). Multirotor aerial vehicles: Modeling, estimation, and control of quadrotor. *IEEE Robot. Autom. Mag.*, *19*(3), 20–32. doi: 10.1109/MRA.2012.2206474

McKerrow, P. (2004). Modelling the Draganflyer four-rotor helicopter. In *Proc. - ieee int. conf. robot. autom.* (Vol. 4, pp. 3596–3601 Vol.4). IEEE. Retrieved from http://ieeexplore.ieee.org/document/1308810/ doi: 10.1109/ROBOT.2004.1308810

Mendes, a. S., Kampen, E. V., & Chu, Q. P. (2012). Determining moments of inertia of small UAVs : A comparative analysis of an experimental method versus theoretical approaches. In *Aiaa guid. navig. control conf.* (pp. 1–14). doi: doi:10.2514/6.2012-4463

Merwe, R. V. D., & Wan, E. a. (2004). Sigma-Point Kalman Filters for Integrated Navigation. In *Proc. annu. meet. - inst. navig.* (pp. 641–654). Retrieved from http://citeseerx.ist.psu.edu/viewdoc/download?doi=10.1.1.9.5753{&}rep=rep1{&}type=pdf doi: 10.1.1.9.5753

Mills, M. P. (2016, mar). *Drone Disruption: The Stakes, The Players, And The Opportunities.* Retrieved 2017-06-22, from https://www.forbes.com/sites/markpmills/2016/03/23/drone-disruption-the-stakes-the-players-and-the-opportunities/ https://www.forbes.com/sites/markpmills/2016/03/23/drone-disruption-the-stakes-the-players-and-the-opportunities/{#}ed8a2fe7d0b5

Mitchell, I., Bayen, A., & Tomlin, C. (2005, jul). A time-dependent Hamilton-Jacobi formulation of reachable sets for continuous dynamic games. *IEEE Trans. Automat. Contr.*, *50*(7), 947–957. Retrieved from http://ieeexplore.ieee.org/document/1463302/ doi: 10.1109/TAC.2005.851439

Mueller, M. W., & D'Andrea, R. (2014, may). Stability and control of a quadrocopter despite the complete loss of one, two, or three propellers. In *2014 ieee int. conf. robot. autom.* (pp. 45–52). IEEE. Retrieved from http://ieeexplore.ieee.org/document/6906588/ doi: 10.1109/ICRA.2014.6906588

Mulder, J. A. (1986). *Design and evaluation of dynamic flight test manoeuvres* (Tech. Rep.). Retrieved from http://repository.tudelft.nl/islandora/object/uuid:a6d75095-1908-472a-9d7b-cfdf313908fd/datastream/OBJ/view

Norouzi Ghazbi, S., Aghli, Y., Alimohammadi, M., & Akbari, A. A. (2016). Quadrotors unmanned aerial vehicles: A review. *Int. J. Smart Sens. Intell. Syst.*, *9*(1), 309–333.

Paparazzi Repository. (n.d.). Retrieved 2018-06-14, from https://github.com/paparazzi/paparazzi/

Paparazzi Wiki. (n.d.). Retrieved 2018-06-14, from https://wiki.paparazziuav.org/wiki/Main{_}Page

Pounds, P., Mahony, R., & Corke, P. (2007, feb). System Identification and Control of an Aerobot Drive System. In *Conf. proc. 2007 information, decis. control. idc* (pp. 154–

159). IEEE. Retrieved from http://ieeexplore.ieee.org/document/4252494/ doi: 10.1109/IDC.2007.374542

Powers, C., Mellinger, D., Kushleyev, A., Kothmann, B., & Kumar, V. (2013). Influence of Aerodynamics and Proximity Effects in Quadrotor Flight. In *Springer tracts adv. robot. - exp. robot.* (Vol. 88, pp. 289–302). Retrieved from http://link.springer.com/chapter/10.1007/978-3-319-00065-7{_}21 doi: 10.1007/978-3-319-00065-7

Shah, G., Foster, J., & Cunningham, K. (2010, aug). Simulation Modeling for Off-Nominal Conditions - Where Are We Today? In *Aiaa model. simul. technol. conf.* Reston, Virigina: American Institute of Aeronautics and Astronautics. Retrieved from https://ntrs.nasa.gov/search.jsp?R=20100033316http://arc.aiaa.org/doi/10.2514/6.2010-7792 doi: 10.2514/6.2010-7792

Smeur, E., Chu, Q., & De Croon, G. (2016). Adaptive incremental nonlinear dynamic inversion for attitude control of micro air vehicles. *J. Guid. Control. Dyn.*, *39*(3). doi: 10.2514/1.G001490

Smith, P. (1998). A simplified approach to nonlinear dynamic inversion based flight control. In *23rd atmos. flight mech. conf.*

Stapel, J., de Visser, C. C., Van Kampen, E.-J., & Chu, Q. P. (2016, jan). Efficient Methods for Flight Envelope Estimation through Reachability Analysis. In *Aiaa guid. navig. control conf.* Reston, Virginia: American Institute of Aeronautics and Astronautics. Retrieved from http://arc.aiaa.org/doi/10.2514/6.2016-0083 doi: 10.2514/6.2016-0083

Visser, T., De Visser, C. C., & Van Kampen, E.-J. (2015). *Quadrotor System Identification Using the Multivariate Multiplex B-Spline* (No. January). AIAA. doi: doi:10.2514/6.2015-0747

Wan, E., & Van Der Merwe, R. (2000). The unscented Kalman filter for nonlinear estimation. In *Proc. ieee 2000 adapt. syst. signal process. commun. control symp.* (pp. 153–158). IEEE. Retrieved from http://ieeexplore.ieee.org/document/882463/ doi: 10.1109/ASSPCC.2000.882463

Wei, W., Schwartz, N., & Cohen, K. (2014, jan). Frequency-Domain System Identification and Simulation of a Quadrotor Controller. In *Aiaa model. simul. technol. conf.* Reston, Virginia: American Institute of Aeronautics and Astronautics. Retrieved from http://arc.aiaa.org/doi/10.2514/6.2014-1342 doi: 10.2514/6.2014-1342

Zhang, X., Li, X., Wang, K., & Lu, Y. (2014). A Survey of Modelling and Identification of Quadrotor Robot. *Abstr. Appl. Anal.*, *2014*, 1–16. Retrieved from http://www.hindawi.com/journals/aaa/2014/320526/ doi: 10.1155/2014/320526

Zhang, Y., de Visser, C. C., & Chu, Q. P. (2016, jan). Online Physical Model Identification for Database-driven Safe Fight Envelope Prediction of Damaged Aircraft. In *Aiaa atmos. flight mech. conf.* (pp. 1–11). Reston, Virginia: American Institute of Aeronautics and Astronautics. Retrieved from http://arc.aiaa.org/doi/10.2514/6.2016-2011 doi: 10.2514/6.2016-2011